

1
2
3
4
5
6
7
8
9
10
11
12
13
14
15
16
17
18
19
20
21
22
23
24
25
26
27
28
29
30

Figure or Table # Please group Extended Data items by type, in sequential order. Total number of items (Figs. + Tables) must not exceed 10.	Figure/Table title One sentence only	Filename Whole original file name including extension. i.e.: Smith_ED_Fig1.jpg	Figure/Table Legend If you are citing a reference for the first time in these legends, please include all new references in the main text Methods References section, and carry on the numbering from the main References section of the paper. If your paper does not have a Methods section, include all new references at the end of the main Reference list.
Extended Data Fig. 1	Chemotactic response of <i>Marinobacter adhaerens</i> HP15 to metabolites exuded by <i>Synechococcus</i>	Raina_ED_Fig1.eps	The chemotactic index, I_c denotes the concentration of cells within ISCA wells, normalized by the mean concentration of cells within wells containing no chemoattractants (filtered ESAW), after 30 min laboratory deployment. Wells containing <i>Synechococcus</i> exudates (1 mg ml^{-1}) and 10% Marine Broth (MB) contained significantly more bacteria than the ESAW control (ANOVA, $n = 5$ biologically independent samples, $p < 0.005$; Table S5). Error bars represent standard error of the mean.
Extended Data Fig. 2	Dissolved Organic Matter (DOM) exposure of model bacteria	Raina_ED_Fig2.eps	Mean DOM exposure for three bacterial motility strategies across three different <i>Synechococcus</i> concentrations (leakage rate $L = 0.052 \text{ pmol hr}^{-1}$). Chemotaxis conferred an enhancement in the DOM exposure by 2.1-, 1.3-, and 1.1-fold, for <i>Synechococcus</i> concentrations of 10^3 , 10^4 , and $10^5 \text{ cells ml}^{-1}$ respectively, compared to non-chemotactic ($\Delta cheA$) or non-motile ($\Delta fliC$) mutants.
Extended Data Fig. 3	Residence time of model bacteria	Raina_ED_Fig3.eps	(a) . The bacterial residence time depends on the radius of the analysis zone and motility strategy. For $\Delta cheA$ mutants, the residence time grows linearly with radius. However, WT cells exhibit a steep increase for small radii, reflecting their capacity to detect the phytoplankton exudates. (b) The rate at which the residence time increases with radius reveals the zone in which chemotactic bacteria exhibit the strongest behavioral response to the DOM gradient. From this the encounter radius of $35 \mu\text{m}$ can be extracted. Other

			model parameters include $L = 0.052 \text{ pmol hr}^{-1}$, $\rho = 10^3 \text{ cells ml}^{-1}$.
Extended Data Fig. 4	DOM profile does not depend strongly on bacterial consumption	Raina_ED_Fig4.ep s	In each plot, the steady state DOM profile emerges due to a balance between constant phytoplankton exudation and diffusion-limited uptake by bacteria. (a) DOM profile for four different bacterial concentrations. (b) Restricting bacteria to lie in the region $R < R_0$ has a minor influence on the resultant DOM profile.
Extended Data Fig. 5	Growth of <i>Synechococcus</i> sp. CS-94 RRIMP N1 and <i>Marinobacter adhaerens</i> HP15	Raina_ED_Fig5.ep s	(a) Growth curves of <i>M. adhaerens</i> HP15 wild type (WT), non-chemotactic mutant ($\Delta cheA$), and non-motile mutant ($\Delta fliC$), each separately co-cultured with <i>Synechococcus</i> at an initial concentration of $10^3 \text{ cells ml}^{-1}$ for both partners. (b) Simultaneous growth curve of <i>Synechococcus</i> for the same three co-culture experiments. Note: to clearly visualise differences in cell numbers during early timepoints, <i>Synechococcus</i> cell numbers are plotted on a logarithmic scale. Asterisks indicate timepoints at which treatments are significantly different (simple main effect test, $p < 0.05$, Table S9). Error bars represent standard error of the mean ($n = 4$ biologically independent samples). (c) Growth curves of <i>Marinobacter adhaerens</i> HP15 wild type (WT), non-chemotactic mutant ($\Delta cheA$), and non-motile mutant ($\Delta fliC$) in Marine Broth. Error bars represent standard error of the mean ($n = 3$ biologically independent samples). Asterisks indicate timepoints at which treatments are significantly different (simple main effect test, $p < 0.05$, Table S10).
Extended Data Fig. 6	DOM concentration within a 2D cross-section of the full 3D profile	Raina_ED_Fig6.ep s	Results correspond to a <i>Synechococcus</i> concentration of $\rho = 10^3 \text{ cells ml}^{-1}$. Other parameters as in Table S8. The white scale bar represents 1 mm.

Extended Data Fig. 7	DOM exposure of model bacteria	Raina_ED_Fig7.ep s	The mean DOM concentration experienced by (a) non-chemotactic ($\Delta cheA$) mutants and (b) chemotactic (WT) bacteria, as a function of phytoplankton concentration (cells ml^{-1}) and DOM leakage rate L (pmol hr^{-1}).
Extended Data Fig. 8	Phytoplankton exudation rate affects bacteria-phytoplankton distances and bacterial “trapping”	Raina_ED_Fig8.ep s	(a) Bacteria-phytoplankton distance is strongly affected by phytoplankton exudation rate. These data show the distance to the nearest hotspot, averaged over time (3 h co-incubation) and bacterial population (500 cells), as a function of DOM leakage rate L (pmol hr^{-1}). Results are shown for three different phytoplankton concentrations, 10^3 (dotted), 10^4 (dashed), 10^5 cells ml^{-1} (solid), and for three different bacterial mutants: chemotactic WT (blue), non-chemotactic $\Delta cheA$ (orange), non-motile $\Delta fliC$ (red). (b) Bacteria-phytoplankton trapping statistics. These data show the percentage of bacterial cells that are situated within $35\ \mu m$ of a phytoplankton cell (phycosphere), as a function of DOM leakage rate L (pmol hr^{-1}). For each datapoint, results have been averaged over time (3 h co-incubation) and bacterial population (500 cells). Results are shown for three different phytoplankton concentrations, 10^3 (dotted), 10^4 (dashed), 10^5 cells ml^{-1} (solid), and for three different bacterial mutants: chemotactic WT (blue), non-chemotactic $\Delta cheA$ (orange), non-motile $\Delta fliC$ (red).
Extended Data Fig. 9	Distribution of the single cell enrichment data reported in Figure 1 and 2	Raina_ED_Fig9.ep s	(a) ^{15}N uptake of <i>M. adhaerens</i> (10^3 : n=166; 10^4 : n=286; 10^5 : n=172) and (b) ^{13}C uptake of <i>Synechococcus</i> (10^3 : n=10; 10^4 : n=17; 10^5 : n=37).
Choose an item.			

Item	Present?	Filename Whole original file name including extension. i.e.: Smith_SI.pdf. The extension must be .pdf	A brief, numerical description of file contents. i.e.: <i>Supplementary Figures 1-4, Supplementary Discussion, and Supplementary Tables 1-4.</i>
Supplementary Information	Yes	Raina_et_al_SI.pdf	Supplementary Figure 1, Supplementary Tables 1-10
Reporting Summary	Yes	nr-reporting-summary_jb_raina_Jan23.pdf	
Peer Review Information	No	OFFICE USE ONLY	

33

34

35

36

Type	Number Each type of file (Table, Video, etc.) should be numbered from 1 onwards. Multiple files of the same type should be listed in sequence, i.e.: Supplementary Video 1, Supplementary Video 2, etc.	Filename Whole original file name including extension. i.e.: <i>Smith_Supplementary_Video_1.mov</i>	Legend or Descriptive Caption Describe the contents of the file
Supplementary Table	Supplementary Tables 1-10	Raina_et_al_SupplementaryTables.xlsx	Full Supplementary Tables 1-10
Choose an item.			
Choose an item.			
Choose an item.			

37

38

Parent Figure or Table	Filename Whole original file name including extension. i.e.: <i>Smith_SourceData_Fig1.xls</i> , or <i>Smith_Unmodified_Gels_Fig1.pdf</i>	Data description i.e.: Unprocessed western Blots and/or gels, Statistical Source Data, etc.
------------------------	---	--

Source Data Fig. 1	Raina_et_al_SourceFig1.xlsx	Raw data for Figure 1
Source Data Fig. 2	Raina_et_al_SourceFig2.xlsx	Raw data for Figure 2

39

40
41 **Chemotaxis increases metabolic exchanges between marine picophytoplankton and**
42 **heterotrophic bacteria**
43

44 Jean-Baptiste Raina^{1*#}, Marco Giardina^{1*}, Douglas R. Brumley^{2*}, Peta L. Clode^{3,4,5},
45 Mathieu Pernice¹, Paul Guagliardo³, Jeremy Bougoure³, Himasha Mendis⁶, Steven Smriga⁷,
46 Eva C. Sonnenschein^{8,9}, Matthias S. Ullrich¹⁰, Roman Stocker¹¹, Justin R. Seymour^{1#}

47

48

49 ¹ University of Technology Sydney, Climate Change Cluster, Faculty of Science, Ultimo,
50 NSW, Australia

51 ² School of Mathematics and Statistics, The University of Melbourne, Parkville, Victoria,
52 Australia,

53 ³ Centre for Microscopy Characterisation and Analysis, The University of Western Australia,
54 Perth, Australia

55 ⁴ UWA School of Biological Sciences, The University of Western Australia, Perth, Australia

56 ⁵ UWA Oceans Institute, The University of Western Australia, Perth, Australia

57 ⁶ Metabolomics Australia, Bio21 Institute, The University of Melbourne, Parkville, Australia

58 ⁷ Department of Earth Atmospheric and Planetary Sciences, Massachusetts Institute of
59 Technology, Cambridge, MA, USA

60 ⁸ Department of Biotechnology and Biomedicine, Technical University of Denmark, Kgs.
61 Lyngby, Denmark

62 ⁹ Department of Biosciences, Swansea University, Singleton Park, Swansea, SA2 8PP,
63 Wales, United Kingdom

64 ¹⁰ Department of Life Sciences & Chemistry, Jacobs University Bremen, Bremen, Germany

65 ¹¹ Institute of Environmental Engineering, Department of Civil, Environmental and Geomatic
66 Engineering, ETH Zurich, Zurich, Switzerland

67

68 * These authors contributed equally to this work

69 # Corresponding authors

70 Jean-Baptiste.Raina@uts.edu.au

71 Justin.Seymour@uts.edu.au

72

73

74 **Abstract**

75 Behaviours such as chemotaxis can facilitate metabolic exchanges between phytoplankton and
76 heterotrophic bacteria, which ultimately regulate oceanic productivity and biogeochemistry.
77 However, numerically dominant picophytoplankton have been considered too small to be
78 detected by chemotactic bacteria, implying that cell-cell interactions might not be possible
79 between some of the most abundant organisms in the ocean. Here we examined how bacterial
80 behaviour influences metabolic exchanges at the single-cell level between the ubiquitous
81 picophytoplankton *Synechococcus* and the heterotrophic bacterium *Marinobacter adhaerens*,
82 using bacterial mutants deficient in motility or chemotaxis. Stable-isotope tracking revealed
83 that chemotaxis increased nitrogen and carbon uptake of both partners by up to 4.4-fold. A
84 mathematical model following thousands of cells confirmed that short periods of exposure to
85 small but nutrient-rich microenvironments surrounding *Synechococcus* cells provide a
86 considerable competitive advantage to chemotactic bacteria. These findings reveal that
87 transient interactions mediated by chemotaxis can underpin metabolic relationships among the
88 ocean's most abundant microorganisms.

89

90 **Main text**

91 The substantial impact of microbial communities on the productivity and biogeochemistry of
92 the ocean is shaped by intricate networks of inter-organismal interactions^{1,2}. Among pelagic
93 microbial relationships, the often-mutualistic metabolic associations between phytoplankton
94 and bacteria are some of the most important^{3,4}. Reciprocal exchanges of metabolites, including
95 a diverse suite of organic and inorganic molecules, vitamins and minerals can support the
96 growth of both phytoplankton and bacterial partners⁵⁻⁷. However, within the vast expanses of
97 the ocean, the efficacy of these, often highly specific, chemical exchanges will be hindered by
98 large inter-cell distances (hundreds of micrometres on average) and the sharp diffusive decay
99 of metabolite concentrations with distance from exuding cells⁸. Phytoplankton-bacteria
100 partnerships may, nevertheless, overcome these constraints through the formation of close
101 spatial associations within the microenvironment immediately surrounding individual
102 phytoplankton cells, known as the phycosphere⁹, which is characterized by elevated
103 concentrations of metabolites emanating from the phytoplankton cell. It has long been
104 theorized⁹⁻¹¹ that bacteria can locate and maintain position within the phycosphere using
105 chemotaxis – the capacity of motile cells to migrate up or down chemical gradients – resulting
106 in sustained spatial proximity of partners¹² and greatly enhanced metabolic exchanges¹³.

107

108 There is substantial evidence for bacterial chemotaxis towards phytoplankton-derived
109 chemicals^{9,12,14,15} and for the ability of bacteria to use chemotaxis to actively aggregate around
110 large phytoplankton cells, such as diatoms¹⁶. Yet, across vast areas of the ocean, phototrophic
111 biomass and primary production are dominated by picophytoplankton (< 3 µm), including
112 picoeukaryotes and the cyanobacteria *Prochlorococcus* and *Synechococcus*¹⁷. Like large
113 phytoplankton including diatoms and dinoflagellates, these picophytoplankton appear to have
114 important metabolic interdependencies with heterotrophic bacteria. Laboratory cultures of
115 *Prochlorococcus* and *Synechococcus* exhibit enhanced growth in the presence of specific
116 heterotrophic associates¹⁸⁻²⁰, and metabolic exchanges have been identified using
117 transcriptomic and proteomic approaches^{18,21}. However, the nature of the ecological coupling
118 between picophytoplankton and heterotrophic bacteria in the environment is somewhat
119 paradoxical. While close proximity of partners is anticipated to strongly enhance and sustain
120 mutualistic phototroph-heterotroph interactions¹², physical constraints associated with the
121 small size of *Prochlorococcus* and *Synechococcus* cells are thought to prevent heterotrophic
122 bacteria from using chemotaxis to detect and retain position within their phycosphere²². Here
123 we show, however, that heterotrophic bacteria are indeed able to utilize chemotaxis to
124 substantially enhance their metabolic exchanges with picophytoplankton, demonstrating that
125 behavioural associations may shape the ecological relationships among some of the oceans'
126 most abundant microorganisms.

127

128 RESULTS

129 *Synechococcus* and *Marinobacter* exchange N and C

130 Using nano-scale secondary ion mass spectrometry (NanoSIMS), we directly quantified the
131 chemical exchanges between *Synechococcus* strain CS-94 RRIMP N1 and *Marinobacter*
132 *adhaerens* HP15, a heterotrophic Gammaproteobacterium associated with larger
133 phytoplankton (diatoms)^{13,23}. Closely related *M. adhaerens* strains (more than 98% 16S rRNA
134 gene sequence identity) are also abundant in picophytoplankton cultures^{20,24}. Given that
135 *Synechococcus* cells produce and release nitrogen-rich dissolved organic matter (DOM) that
136 can be utilised by heterotrophic bacteria¹⁸, we tracked the transfer of nitrogen from
137 *Synechococcus* to *M. adhaerens*. *Synechococcus* cells were grown in f/2 medium with ¹⁵N-
138 labelled NaNO₃ as the only source of nitrogen for one week prior to experiments, to ensure
139 high levels of ¹⁵N enrichment in cells. To facilitate cell localization under NanoSIMS²⁵, *M.*
140 *adhaerens* cells were grown separately with ¹³C-labelled amino acids. *Synechococcus* and *M.*
141 *adhaerens* cells were then thoroughly washed to remove isotopic labels from suspensions and

142 co-grown across a range of *Synechococcus* concentrations (10^3 , 10^4 and 10^5 cells ml $^{-1}$)
143 reflecting those occurring in different environments (from open ocean to coastal waters), with
144 a constant concentration of *M. adhaerens* (10^6 cells ml $^{-1}$). Following three hours of co-
145 incubation in stable light and temperature conditions²⁶, samples were collected for NanoSIMS
146 analysis.

147

148 After co-incubation, *M. adhaerens* cells were enriched in ^{15}N derived from *Synechococcus*,
149 with levels up to 2.7 times the natural abundance values of ^{15}N in unlabelled *M. adhaerens*
150 ($^{15}\text{N}/^{14}\text{N} = 0.010 \pm 0.00081$, $n = 172$, compared to 0.0037 ± 0.000046 , $n = 300$). Significant
151 uptake of *Synechococcus*-derived ^{15}N by *M. adhaerens* (the percentage of N incorporated into
152 the cells relative to the initial N content; see equation (1) in the Methods) occurred at all
153 *Synechococcus* concentrations (Kruskal-Wallis (KW), $p < 0.05$; Table S1). ^{15}N uptake in *M.*
154 *adhaerens* increased strongly with the concentration of *Synechococcus* cells (KW, $p < 0.05$;
155 Table S1), from 0.36% at 10^3 *Synechococcus* cells ml $^{-1}$ to 0.98% at 10^5 *Synechococcus* cells
156 ml $^{-1}$ (Figure 1a-b). These results deliver direct evidence that nitrogen-containing compounds
157 exuded from *Synechococcus* are taken up by heterotrophic bacteria, demonstrating that
158 chemical exchange takes place between these two organisms.

159

160 To identify which organic nitrogen compounds are exuded by *Synechococcus*, we used an
161 untargeted metabolomic approach. We identified 34 nitrogen-containing compounds exuded
162 by *Synechococcus*, using gas chromatography coupled with mass spectrometry (GC-MS). The
163 exuded compounds included amino acids (cysteine, phenylalanine, methionine, leucine),
164 amines (tyramine, ethanalamine), amides (urea), vitamins (nicotinamide, pantothenic acid),
165 and purines (xanthine; Table S2). Notably, an analysis of the *M. adhaerens* HP15 genome²⁷
166 indicates that this bacterium has the capacity to catabolize at least 24 of these 34 compounds
167 (>70%; Table S2), implying the probable importance of these molecules in the metabolic
168 exchange between *Synechococcus* and heterotrophs¹⁸.

169

170 Beyond the transfer of nitrogen from *Synechococcus* to *M. adhaerens*, our analysis also
171 revealed an unexpected exchange of carbon from *M. adhaerens* to *Synechococcus*, evidenced
172 by ^{13}C enrichment in *Synechococcus* cells that reached up to 2.9 times the natural abundance
173 values in unlabelled cells ($^{13}\text{C}/^{12}\text{C} = 0.032 \pm 0.0051$, $n = 10$, compared to 0.011 ± 0.000027 , n
174 = 102). ^{13}C uptake was not affected by the *Synechococcus* concentration (the percentage of C
175 incorporated into the cells relative to the initial C content; see equation (1) in Methods; KW,

176 $p>0.05$; Table S3, Figure 1c-d), likely because no competition for ^{13}C occurred at the
177 *Synechococcus* concentrations tested (see Methods). Using GC-MS, we identified 80 organic
178 compounds exuded by *M. adhaerens* that potentially contributed to the carbon enrichment in
179 *Synechococcus*. These compounds included sugars (galactose, mannose, sucrose), amino acids
180 (glycine, alanine, serine), organic acids (phosphoric acid, benzoic acid, pyroglutamic acid),
181 hormones (methoxytryptamine), and fatty acids (linoleic acid, palmitic acid, myristic acid;
182 Table S4). The identity of some of these compounds is consistent with previous reports of
183 photoheterotrophy in *Synechococcus* and their uptake of amino acids and urea^{28,29}. Taken
184 together, these results provide the first direct evidence that *Synechococcus* cells can
185 simultaneously supply heterotrophic bacteria with nitrogen while acquiring carbon from them
186 (Figure 1e), pointing to a relationship that is akin to the reciprocal metabolic associations
187 observed between larger phytoplankton (*e.g.*, diatoms) and heterotrophic bacteria⁶.

188

189 **Chemotaxis facilitates reciprocal metabolic exchanges**

190 *M. adhaerens* is motile¹³ and we found, using a chemotaxis assay³⁰, that it is significantly
191 attracted towards dissolved organic matter exuded by *Synechococcus* (3.5 ± 0.3 times more
192 cells compared to controls, which consistent with levels of chemoattraction reported for other
193 marine Gammaproteobacteria the same experimental conditions³¹; ANOVA, $p<0.05$; Table S5,
194 Extended Data Figure 1). However, this observation does not provide confirmation that *M.*
195 *adhaerens* can use chemotaxis to home in on the phycosphere of individual *Synechococcus*
196 cells to gain a metabolic benefit. In fact, a previous mathematical model (parameterized with
197 the chemosensory capabilities of *Escherichia coli*), predicted that the chemical gradients in the
198 phycosphere of picophytoplankton are too small to be detectable by chemotactic bacteria²².
199 This prediction has resulted in the paradigm that, whereas associations between heterotrophic
200 bacteria and large phytoplankton can be mediated by bacterial behaviour^{11,22}, those between
201 heterotrophic bacteria and picophytoplankton cannot²². To explicitly test the role of chemotaxis
202 in the exchange of resources between the two microorganisms, we compared the uptake of
203 *Synechococcus*-derived ^{15}N by *M. adhaerens* among three *M. adhaerens* phenotypes: the
204 motile and chemotactic wild-type (WT); a motile but non-chemotactic mutant (ΔcheA)¹³; and
205 a non-motile mutant (ΔfliC)¹³ (Figure 2a).

206

207 These experiments revealed that the magnitude of the chemical exchange between
208 *Synechococcus* and *M. adhaerens* was substantially smaller when *M. adhaerens* cells were not
209 chemotactic. After three hours of co-incubation with ^{15}N -labelled *Synechococcus*, bacteria

210 from all three phenotypes were enriched in ^{15}N compared to unlabelled cells (Figure 2b), but
211 the level of enrichment was strongly determined by the bacteria's capacity for chemotaxis.
212 Specifically, in the treatments with the low and intermediate *Synechococcus* concentrations
213 (10^3 and 10^4 cells ml^{-1}), the ^{15}N uptake of the WT *M. adhaerens* was more than double that of
214 the $\Delta fliC$ (2.6 and 2.4-fold increase, for 10^3 and 10^4 cells ml^{-1} , respectively) and $\Delta cheA$ (2.0
215 and 1.8-fold increase, for 10^3 and 10^4 cells ml^{-1} , respectively) mutants (KW, $p<0.05$; Table S6,
216 Figure 2b). At high *Synechococcus* concentrations (10^5 cells ml^{-1}) this difference vanished,
217 possibly because a high background concentration of substrates renders chemotaxis less
218 advantageous. These results overturn the paradigm that chemotaxis of heterotrophic bacteria
219 towards picophytoplankton is not possible, showing instead that it can deliver bacteria with a
220 substantial advantage in metabolic uptake.

221
222 Chemotaxis of *M. adhaerens* also influenced the uptake of *M. adhaerens*-derived organic
223 carbon by *Synechococcus*. At concentrations of 10^4 and 10^5 cells ml^{-1} , *Synechococcus* co-
224 incubated with WT *M. adhaerens* were up to four times more enriched in ^{13}C than cells co-
225 incubated with $\Delta fliC$ (1.2 and 1.5-fold increase, for 10^4 and 10^5 cells ml^{-1} , respectively) and
226 $\Delta cheA$ (1.8 and 4.4-fold increase, for 10^4 and 10^5 cells ml^{-1} , respectively) mutants (KW,
227 $p<0.001$; Table S7, Figure 2c). Therefore, chemotaxis by heterotrophic bacteria not only
228 enhances the uptake of picophytoplankton-derived metabolites by the bacteria, but also
229 increases picophytoplankton uptake of bacteria-derived metabolites, identifying chemotaxis as
230 an important behaviour in the establishment of reciprocal resource exchange between two of
231 the most numerous groups of microorganisms in the ocean.

232
233 **Phycosphere interactions are short-lived yet repeated**
234 The role of chemotaxis in enhancing bacterial uptake of picophytoplankton metabolites was
235 supported by a mathematical model that simulates the motion of chemotactic bacteria in a
236 three-dimensional dissolved organic matter (DOM) landscape representative of experimental
237 conditions. A suspension of *Synechococcus* cells was modelled as a collection of randomly
238 positioned spherical 'hotspots', each exuding DOM at a steady rate $L = 0.052 \text{ pmol h}^{-1}$, which
239 was determined by calibrating the model with experimental parameters (see Methods, Table
240 S8) and is consistent with predictions based on previous estimates of phytoplankton exudation
241 rates¹². Based on the high proportion of amino acids we measured in the *Synechococcus*
242 exudates by metabolomics (Table S2), the DOM was represented in the model as a single
243 chemoattractant molecule of amino-acid size (diffusivity: $608 \mu\text{m}^2 \text{s}^{-1}$)³². The model predicted

244 how the DOM concentration changes in space and time as a result of exudation, diffusion and
245 bacterial uptake, and used this information to compute the three-dimensional trajectories of
246 bacteria executing run-reverse-flick locomotion representative of monotrichous marine
247 bacteria^{22,32}. The amount of DOM taken up by 500 individual *M. adhaerens* cells (at 10⁶ cells
248 ml⁻¹) was calculated over three hours (see Methods), for the same three bacterial phenotypes
249 (WT, $\Delta cheA$, $\Delta fliC$) used in the experiments. Results revealed an increased uptake of DOM by
250 WT cells when compared to both $\Delta cheA$ and $\Delta fliC$ mutants (Extended Data Figure 2), in
251 agreement with experimental results (Figure 2b). Specifically, chemotactic cells (WT)
252 exhibited a 2.1-, 1.3-, and 1.1-fold increase in DOM uptake over the $\Delta cheA$ mutants, for
253 *Synechococcus* concentrations of 10³, 10⁴, and 10⁵ cells ml⁻¹, respectively.

254

255 Investigation of individual bacterial trajectories from the mathematical model revealed the
256 fleeting nature of the interactions between bacteria and picophytoplankton. We defined the
257 phycosphere radius, $R_p = 35 \mu\text{m}$, as the distance from individual *Synechococcus* cells at which
258 the bacterial chemotactic response was strongest (see Methods; Extended Data Figure 3). This
259 allowed us to quantify from the model the residence time τ associated with each encounter of
260 a bacterium with a *Synechococcus* phycosphere (Figure 3), defined as the time between entry
261 to and departure from the phycosphere (Figure 3a). Computing the residence time for all
262 bacteria-phycosphere encounters revealed that WT cells spend on average three times longer
263 in *Synechococcus* phycospheres ($\tau=3.2\pm11.5$ s, $n=82,242$ encounters) than $\Delta cheA$ mutants
264 ($\tau=1.0\pm1.4$ s, $n=2,626$ encounters; Figure 3b-c). The difference was even more pronounced for
265 longer encounters, with residence times greater than 10 s being 16 times more likely for WT
266 cells (7.3% of encounters) than for $\Delta cheA$ mutants (0.46% of encounters).

267

268 Beyond the duration of individual encounters, our trajectory analysis revealed that chemotaxis
269 strongly affects the number of unique phycosphere encounters per day. At a *Synechococcus*
270 concentration of 10³ cells ml⁻¹, chemotaxis more than tripled the mean encounter rate of
271 bacteria with phycospheres (WT: 12.6 day⁻¹; $\Delta cheA$: 4.1 day⁻¹; Figure 3d). The distribution of
272 encounters revealed that 29% of WT cells but only 0.7% of $\Delta cheA$ cells encountered more than
273 15 unique phycospheres per day. Moreover, the top 5% of WT cells encountered on average
274 36 unique phycospheres per day, compared to only 13 for the top 5% of $\Delta cheA$ cells (Figure
275 3d).

276

277 The phycosphere afforded WT bacteria a substantial fraction of their uptake, even though time
278 spent in the phycosphere was short. Our model revealed that WT bacteria derived 30% of their
279 total DOM uptake from the phycosphere, despite spending merely 1.7% of time in it. In stark
280 contrast, for $\Delta cheA$ bacteria, the proportion of DOM uptake originating from the phycospheres
281 was ~100-fold smaller – they derived just 0.38% of their DOM uptake from the phycosphere,
282 where they spent only 0.02% of time. We conclude that the differences in residence time,
283 coupled with the sharp spatial decay of the DOM concentration in the phycosphere (Extended
284 Data Figure 4), is the cause of the significant enhancement in DOM uptake conferred by
285 chemotaxis.

286

287 **Chemotaxis provides growth advantages**

288 To further explore how chemotactic behaviour may affect the fitness of heterotrophic bacteria,
289 we conducted a multi-day co-culture experiment between *Synechococcus* and each of the three
290 *M. adhaerens* phenotypes (at a starting concentration of 10^3 cells ml $^{-1}$ for both partners). Our
291 results demonstrate that WT *M. adhaerens* grew significantly faster in co-culture with
292 *Synechococcus* than the non-motile mutant and the non-chemotactic mutant (repeated measure
293 ANOVA, $p < 0.05$; Table S9, Extended Data Figure 5). This effect was sustained over four
294 days while *Synechococcus* concentrations remained low, but disappeared as *Synechococcus*
295 increased in abundance beyond 10^5 cell ml $^{-1}$ (Extended Data Figure 5). Importantly, this growth
296 enhancement occurred despite both $\Delta cheA$ and $\Delta fliC$ mutants growing significantly faster than
297 the WT under nutrient-replete conditions (repeated measure ANOVA, $p < 0.05$; Table S10,
298 Extended Data Figure 5). These results reveal that the greater nutrient uptake achieved by
299 chemotactic cells over short timescales (minutes to hours) ultimately increases cell fitness over
300 longer timescales (days).

301

302 Our numerical simulations allowed us to extend the analysis to phytoplankton cells of different
303 sizes, and explore the relative advantage provided by chemotaxis across a range of realistic
304 nutrient sources (Figure 4). Indeed, our simulations revealed that the advantage of chemotaxis
305 is most pronounced at low phytoplankton concentrations, regardless of the phytoplankton cell
306 sizes (or equivalently nutrient leakage rate). However, the relative advantage provided by
307 chemotaxis increased with phytoplankton size, with a >50-fold enhancement in DOM exposure
308 over $\Delta cheA$ mutants when interacting with large, but widely separated phytoplankton (Figure
309 4). In addition, larger phytoplankton sizes dramatically increase the mean residence time of
310 chemotactic bacteria (Figure 3c), ultimately suppressing the transient interactions reported for

311 *Synechococcus* and limiting bacterial dispersal (Figure 3e-f). These data indicate qualitatively
312 distinct bacterial interactions with small and large phytoplankton, respectively, and can serve
313 as a blueprint for studying ecological interactions in different regimes.

314

315 Our experiments were carried out in laboratory conditions whereby cells were suspended in a
316 nitrogen and phosphorous-rich medium, which is not directly reflective of the nutrient-limiting
317 conditions prevailing in the oligotrophic ocean, and this could potentially influence rates of
318 exudation by *Synechococcus* cells. The factors governing the exudation rates of organic
319 substrates from phytoplankton cells are still largely unresolved¹², and ambient nutrient levels
320 may potentially influence exudation rates. While some evidence suggests that exudation rates
321 are enhanced in oligotrophic conditions³³, it is also possible that under nutrient-limited
322 conditions *Synechococcus* cells may reduce the amount of nitrogen they exude. This
323 uncertainty notwithstanding, our numerical simulations indicate that even if the leakage rate of
324 *Synechococcus* cells were substantially smaller than the one observed in our experiments (i.e.
325 $L=0.01 \text{ pmol h}^{-1}$), the relative enhancement in nutrient exposure due to chemotaxis would still
326 be sizeable (e.g. 11% enhancement if the exudation rate was five times smaller; Figure 4).

327

328 DISCUSSION

329 The principal goal of our study was to determine whether chemotaxis enhances heterotrophic
330 bacterial exposure to, and assimilation of, substrates released into the phycosphere by
331 picophytoplankton. Motility comes at an energetic cost for cells³⁴, which we have here not
332 explicitly considered. This energetic cost would partly offset the nutrient uptake advantage and
333 could result in there being a *Synechococcus* cell concentration below which motility no longer
334 provides an advantage. However, in our experiments, no significant difference in ¹⁵N uptake
335 between non-chemotactic and non-motile cells was recorded over short co-incubations (Figure
336 2b), suggesting that the energetic cost of swimming was not detectable over that timeframe (3
337 hours). However, during longer co-incubations (12 days), the non-motile cells grew on average
338 24.5% faster than the non-chemotactic ones (Extended Data Figure 5), potentially due to the
339 cost of building and operating the flagellar apparatus.

340

341 Taken together, our experimental and modelling results both (i) provide the first quantitative
342 demonstration that chemotaxis enhances the uptake of phytoplankton-derived metabolites by
343 motile heterotrophic marine bacteria and (ii) overturns the paradigm (previously based on the
344 chemotactic parameters from *E. coli*²²) that marine bacteria will not be able to use chemotaxis

345 towards individual picophytoplankton. The latter points to a greater chemotactic sensitivity of
346 marine bacteria compared to *E. coli*, which is in line with prior observations on the chemotaxis
347 of marine bacteria^{32,35}. Picophytoplankton collectively amount to a biomass similar to diatoms
348 at the global scale (12.7 and 16.5 µg C L⁻¹, respectively)³⁶, despite their diameter being 10-
349 100-fold smaller³⁶, and are the dominant phototrophic organisms in many parts of the
350 oligotrophic ocean¹⁷. Our findings therefore expand the potential for chemotaxis to govern the
351 ecological and metabolic interactions between heterotrophic bacteria and phytoplankton to a
352 major fraction of phototrophic biomass in the ocean.

353

354 Our results show that chemotactic bacteria benefit from phytoplankton not just by migrating
355 into and retaining position within their phycosphere, as occurs for larger phytoplankton¹⁶, but
356 through transient spatial associations with the phycospheres. These brief encounters still
357 provide conspicuous advantages, because spending even a small fraction of time in the highly
358 DOM-enriched vicinity of phytoplankton cells translates into large increases in DOM uptake¹⁶.
359 Because of the abundance of picophytoplankton in the global ocean¹⁷, these fleeting
360 interactions will be numerous, providing a viable strategy for nutrient exchanges in the water
361 column. Rather than stably associating with *Synechococcus*, chemotactic heterotrophs
362 therefore derive a competitive advantage over their non-chemotactic counterparts because they
363 can considerably extend the frequency and duration of their spatial association with
364 picophytoplankton, even if each encounter is highly transient.

365

366 Our experiments reveal that these transient interactions increase not only the uptake of
367 *Synechococcus*-derived dissolved organic nitrogen by heterotrophs, but also the uptake of
368 heterotroph-derived carbon by *Synechococcus* cells. This indicates that chemotactic behaviour
369 can foster reciprocal metabolic exchange between marine microorganisms and thereby
370 potentially enhance primary and secondary production levels and rates of nutrient recycling,
371 even in the large regions of ocean dominated by small phytoplankton cells. Chemotaxis is
372 recognized as a pervasively important behaviour enabling the onset and maintenance of
373 symbiotic interactions across different hosts and environments¹⁴, however, symbiosis
374 commonly refers to spatially close and temporally extended interactions between organisms³⁷.
375 Although very different from this traditional view, the short-lived yet repeated encounters
376 described here benefit both partners and may contribute to their survival in the resource-poor
377 open ocean. These partnerships might therefore represent “transient” symbioses, at the opposite
378 end of obligate intracellular associations on the symbiotic continuum. Together, these

379 observations suggest that even across the large areas of the ocean where phototrophic biomass
380 is dominated by very small cells, sophisticated metabolic interactions among the plankton,
381 facilitated by microbial foraging behaviours, can influence oceanic productivity and
382 biogeochemical cycling. Furthermore, our quantification of the benefits of chemotactic
383 interactions between very small cells highlights that chemotaxis may play an unexpected role
384 in the metabolic exchanges between individual bacterial cells across all environments.

385

386 METHODS

387 *Cultures*

388 *Synechococcus* sp. CS-94 RRIMP N1³⁸ was grown in Enriched Seawater Artificial Water
389 (ESAW)³⁹ complemented with f/2 nutrients⁴⁰. The cells were maintained at 23°C on a 12:12 h
390 dark:light cycle at ~ 180 µmol photons m⁻² s⁻¹. In addition, we used the wild type (WT) marine
391 bacterium *Marinobacter adhaerens* HP15⁴¹ (both motile and chemotactic), $\Delta cheA$ a motile but
392 non-chemotactic mutant¹³, and $\Delta fliC$ a non-motile mutant⁴². In $\Delta cheA$ or $\Delta fliC$ mutants, the
393 genes *cheA* or *fliC*, respectively, were replaced by a chloramphenicol resistance cassette using
394 homologous recombination on the up- and downstream regions of the genes, as described
395 previously^{13,42}. Both mutants were complemented with medium-copy number plasmids
396 (pBBR1MCs-based) containing *cheA* or *fliC*, downstream of the *lac* promoter of the vector.
397 This was needed since neither of these two genes carry their own promoter. These
398 complemented mutants were tested in the respective assays with 10-fold diluted MB 0.3% soft
399 agar (for *cheA* mutant transformant) and the MB 0.3% soft agar assay (*fliC* mutant
400 transformant), showing restoration of wild type levels of motility.

401

402 To determine the growth dynamics of the three *M. adhaerens* HP15 phenotypes (WT, $\Delta cheA$
403 and $\Delta fliC$), single colonies were picked from Marine Agar plates (Difco Laboratories,
404 Michigan) and resuspended in Marine Broth (Difco Laboratories, Michigan). Cell
405 concentrations were quantified using flow cytometry (CytoFLEX S, using CytExpert Version
406 2.4, Beckman Coulter, California), using filtered MilliQ water as the sheath fluid and a flow
407 rate of 25 µl min⁻¹. Cells were fixed with glutaraldehyde (final conc. 2%) and then stained with
408 SYBR Green (final conc. 1:10,000) for 15 minutes in the dark⁴³. For each sample, forward
409 scatter (FSC), side scatter (SSC), green (488 nm, SYBR) and red (650 nm) fluorescence were
410 recorded. *Marinobacter* cells were characterized according to SSC and SYBR Green
411 fluorescence⁴⁴. Flow cytometric counts were used to normalize the starting concentration of

412 *Marinobacter* cells (WT, $\Delta cheA$ and $\Delta fliC$, n=3 for each treatment) to 10,000 cells ml⁻¹ in
413 Marine Broth (Difco Laboratories, Michigan). Cells were incubated at 23°C with shaking (180
414 rpm) and 100 μ l were sampled every two hours from each culture. Cells were then immediately
415 fixed with glutaraldehyde and enumerated as outlined above. To enumerate cell concentrations
416 in each treatment over a 24-hour period, triplicate starting cultures for each treatment were set
417 up twice 12 hours apart. The first set of cultures was enumerated for the first 10 hours, and 12
418 hours later, the second set of cultures was enumerated between 10 and 24 hours.

419

420 ***Isotope labelling***

421 To quantify the reciprocal exchanges of nutrients between *Synechococcus* and *M. adhaerens*,
422 the cells were pre-labeled with the stable isotopes ¹⁵N and ¹³C, respectively. *Synechococcus*
423 cells were inoculated into ESAW complemented with f/2 with ¹⁵N-labeled sodium nitrate
424 (NaNO₃, ¹⁵N, 98 %+, Cambridge Isotopes Laboratories, Massachusetts) as sole source of
425 nitrogen (0.882 mM; same concentration as f/2). The cells were grown in 50 ml for one week,
426 under the same conditions as above, to ensure high level of ¹⁵N enrichment in the cells. Two
427 days before the experiment, glycerol stocks of the three *M. adhaerens* phenotypes were
428 streaked onto respective Difco 2216 Marine Agar plates (Difco Laboratories, Michigan) and
429 incubated at 30°C. The day before the experiment, single colonies of each of the *Marinobacter*
430 phenotypes were suspended into ESAW medium enriched with ¹³C-labeled amino-acids (1 g l⁻¹
431 ¹ Celtone Base Powder; 98%+ ¹³C, Cambridge Isotope Laboratories, Massachusetts) and grown
432 for 12 h at 30°C with shaking (180 rpm), to ensure that the three *Marinobacter* phenotypes
433 were in the same growth phase prior to the start of the experiment. Note: *M. adhaerens* HP15
434 lacks all genes required for dissimilatory or assimilatory nitrate reduction based on its genome
435 annotation (<https://www.genome.jp/entry/gn:T01922>).

436

437 ***Experimental conditions***

438 On the day of the experiment, both *Synechococcus* and *M. adhaerens* cells were rinsed three
439 times to remove all residual stable isotopes from their respective media. Specifically,
440 *Synechococcus* cells were centrifuged at 1,500 g for 15 minutes, the supernatant was discarded
441 and replaced with fresh f/2 medium containing natural abundances of ¹⁵N. These washing steps
442 were performed three times before resuspending the cells in 50 ml of f/2. These repeated media
443 exchanges (from ¹⁵N enriched f/2 to natural abundance) were carried out to ensure that no
444 enriched level of ¹⁵NaNO₃ was present in the growth medium when the co-incubation started.

445 The same washing procedure was applied to the overnight *Marinobacter* cultures to remove
446 ^{13}C from the medium before inoculation.

447

448 The cell concentrations of both *Synechococcus* and the three *Marinobacter* phenotypes were
449 then determined by flow cytometry (CytoFLEX S, Beckman Coulter, California), using filtered
450 MilliQ water as the sheath fluid and a flow rate of 25 $\mu\text{l min}^{-1}$. Cells were fixed with
451 glutaraldehyde (final conc. 2%) for 15 minutes. Prior to analysis, the *Marinobacter* samples
452 were stained with SYBR Green (final conc. 1:10,000) for 15 minutes in the dark⁴³. For each
453 sample, forward scatter (FSC), side scatter (SSC), green (488 nm, SYBR) and red (650 nm)
454 fluorescence were recorded (Figure S1). *Marinobacter* cells were characterized according to
455 SSC and SYBR Green fluorescence⁴⁴, while *Synechococcus* were discriminated according to
456 SSC and red fluorescence (through the autofluorescence of photosynthetic pigments). Cell
457 counts were used to adjust the *Synechococcus* densities to three discrete concentrations: 1,000;
458 10,000; and 100,000 cells ml^{-1} . Each of the three strains of *M. adhaerens* were inoculated
459 separately at a final concentration of 10^6 cells ml^{-1} in each *Synechococcus* cell density.

460

461 *Synechococcus* and *M. adhaerens* strains were co-incubated in triplicates for three hours (based
462 on pilot studies), during the light cycle, under the same light and temperature conditions used
463 for maintaining *Synechococcus*. At the end of the experiment, samples were fixed with
464 glutaraldehyde (final conc. 2%) for 30 minutes. A *Synechococcus* culture maintained in natural
465 abundance of ^{15}N , and a *M. adhaerens* culture maintained in natural abundance of ^{13}C were
466 used as unlabeled controls, these cells were treated identically to all other experimental
467 cultures. To remove any residual glutaraldehyde, the samples were washed with ESAW after
468 pelleting the cells by centrifugation (1,500 g for 15 minutes). Finally, the cells were
469 resuspended in 50 μl of sterile filtered MilliQ water (to remove ESAW salts) and the full
470 volume was immediately placed onto silicon wafers (7.07 mm \times 7.07 mm, Type P / <111>,
471 ProSciTech), dried at 45°C and stored inside a desiccator, protected from light until NanoSIMS
472 analysis. Finally, the samples were coated with 5 nm of gold before being loaded in the
473 NanoSIMS.

474

475 *NanoSIMS analysis*

476 We used the NanoSIMS 50 (Cameca, Gennevilliers, France) at the Centre for Microscopy,
477 Characterisation and Analysis (CMCA) at The University of Western Australia. This
478 instrument allows for simultaneous collection of up to five isotopic species (here: $^{12}\text{C}_2^-$, $^{12}\text{C}^{13}\text{C}^-$

, $^{12}\text{C}^{14}\text{N}^-$, $^{12}\text{C}^{15}\text{N}^-$, ^{32}S). Enrichment of the rare isotopes ^{15}N and ^{13}C was confirmed by an increase in the $^{15}\text{N}/^{14}\text{N}$ or $^{13}\text{C}/^{12}\text{C}$ ratio above the natural abundance value recorded in the control (equal to 0.003716 ± 0.00005 for nitrogen in *Marinobacter* cells and 0.011167 ± 0.000027 for carbon in *Synechococcus* cells). The NanoSIMS was performed using a chain analysis: samples were pre-sputtered for 3.5 minutes at 500 pA Cs^+ beam ($D1=1$) on $30 \mu\text{m}^2$ areas (256×256 pixel), followed by automatic horizontal and vertical secondary ion beam centering. The analysis was then performed by rastering a 2 pA beam ($D1=2$) over $25 \mu\text{m}^2$ areas (256×256 pixels); three planes were recorded per area with a dwell time of 3 ms per pixel. The instrument was operated with a high mass resolving power (in the range of 9,000), allowing the separation of isobaric interferences, and was calibrated daily using yeast cells harboring natural abundance of C, N and S. Images were analyzed using the Fiji software package (version 1.53c) (<http://fiji.sc/Fiji>)⁴⁵ combined with the OpenMIMS plug-in (<http://nrims.harvard.edu/software>). All images were dead-time corrected⁴⁶, the individual planes were then summed prior to extracting counts from the images. Isotopic quantification data were extracted from the mass images by manually drawing regions of interest around each bacterial cell using the $^{12}\text{C}^{14}\text{N}^-$ image as mask. No cell attachment was observed between the two bacterial species in any of the experiments.

496

497 *Calculation of net fixation (uptake)*

498 We converted our NanoSIMS data into percentage of C or N incorporated into the
499 microorganism relative to the initial C or N content, respectively. This net fixation (Fx_{net})⁴⁷ is
500 equal to:

501

$$Fx_{\text{net}} = \frac{R_f \left(1 - \frac{R_i}{R_i + 1}\right) - \frac{R_i}{R_i + 1}}{R_s + 1 - R_f \left(\frac{1}{R_s + 1}\right)} \times 100 \quad (1)$$

502

503 where R_i is the initial isotopic ratios of the organism prior, R_f the final isotopic ratio of the
504 sampled organism, and R_s the isotopic ratios in the pre-enriched partner organism.

505

506 *Characterization of Synechococcus and M. adhaerens HP15 WT metabolites*

507 A 2-liter *Synechococcus* culture was grown for one week in ESAW supplemented with f/2
508 nutrients as described above. A 2-liter *M. adhaerens* culture (WT) was grown overnight as

described above (10% Celtone Base Powder in ESAW; Cambridge Isotope Laboratories, Massachusetts). To characterize the cell exudates, cells were pelleted at 1,500 g for 15 minutes and resuspended individually in fresh ESAW supplemented with f/2 nutrients for three hours. Following this incubation, cells were pelleted at 1,500 g for 15 minutes and the supernatant was filtered through a 0.45 μ m filter, and then through a 0.2 μ m filter to ensure the removal of all cells. The filtrate was acidified to pH 2 using 10% HCl (made with HPLC-water from HCl puriss. 32%, Fluka, Sigma), spiked with internal standards (0.5% final concentration; $^{13}\text{C}_6$ -Sorbitol; ^{13}C - ^{15}N -Valine, penta-fluorobenzoic acid and 2-aminoanthracene) and subjected to a solid phase extraction (SPE; 12 cc, 500 mg sorbent; HLB cartridges, Oasis). After the complete elution of the filtrate, the SPE cartridges were washed twice with 6 ml of 0.01 N HCl to remove residual salts and dried for 20 minutes under vacuum. Finally, the metabolites were eluted with 4 ml of HPLC-grade methanol (Sigma-Aldrich, USA) into glass vials and stored at -20°C until needed.

522

523 *Metabolomics: sample derivatization*

Dried samples for targeted analysis were prepared by adding 25 μ l of Methoxyamine Hydrochloride (30 mg/ml in Pyridine) followed by shaking at 37°C for 2 h. Samples were then derivatized with 25 μ l of *N,O*-bis (Trimethylsilyl)trifluoroacetamide with Trimethylchlorosilane (BSTFA with 1% TMCS, Thermo Scientific) for 1h at 37°C. Samples were left for 1 h before 1 μ l was injected onto the gas chromatography column using a hot needle technique. Split (1:10) injections were done for each sample.

530

531 *Metabolomics: analytical instrumentation*

The gas chromatography–mass spectrometry (GC-MS) system used comprised of an AOC6000 autosampler, a 2030 Shimadzu gas chromatograph and a TQ8050 quadrupole mass spectrometer (Shimadzu, Japan). The mass spectrometer was tuned according to the manufacturer's recommendations using tris-(perfluorobutyl)-amine (CF43). GC-MS was performed on a 30 m Agilent DB-5 column with 1 μ m film thickness and 0.25 mm internal diameter column. The injection temperature (Inlet) was set at 280°C, the MS transfer line at 280°C and the ion source adjusted to 200°C. Helium was used as the carrier gas at a flow rate of 1 ml min⁻¹ and Argon gas was used as the collision cell gas to generate the MRM product ion. Sample analysis was performed under the following temperature program; start at injection 100°C, a hold for 4 minutes, followed by a 10°C min⁻¹ oven temperature ramp to 320°C following final hold off for 11 minutes. Approximately 520 quantifying MRM targets were

543 collected using Shimadzu Smart Database along with qualifier for each target which covers
544 about 350 endogenous metabolites and multiple ^{13}C -labeled internal standards. Both
545 chromatograms and MRMs were evaluated using the Shimadzu GC-MS browser and
546 LabSolutions Insight software. This approach is classified as Level 1-2⁴⁸ or level C according
547 to the proposed reporting standards by the Metabolite Identification Task Group of the
548 Metabolomics Society (<http://metabolomicssociety.org/board/scientific-task-groups/metabolite-identification-task-group>). Resulting area responses were normalized to the
550 internal standard $^{13}\text{C}_6$ Sorbitol area response.

551

552 ***Chemotaxis Assay***

553 To test the chemotactic response of *M. adhaerens* HP15 (WT) towards *Synechococcus*
554 metabolites, we performed a chemotaxis assay using the ISCA (*In Situ* Chemotaxis Assay)³⁰.
555 The ISCA is a microfluidic device composed of an array of microwells which can be filled
556 with different chemoattractants. Here, we used: *i*) ESAW as negative control, *ii*)
557 *Synechococcus* exudates (generated for metabolite analysis above; 1 mg ml⁻¹) and *iii*) 10%
558 Marine Broth (BD Difco) as positive control. Each chemical was resuspended in ESAW and
559 filtered (0.2 μm).

560

561 *Marinobacter adhaerens* HP15 (WT) cells were grown on plate for 3 days. Colonies were then
562 transferred into 0.22- μm -filtered ESAW (room temperature). *M. adhaerens* cells numbers were
563 then adjusted to 10⁶ cells ml⁻¹ with 0.22- μm -filtered ESAW. Each ISCA (n = 5) was deployed
564 in the *M. adhaerens* suspension (80 ml) for 30 minutes⁴⁹. At the end of the incubation, ISCA
565 well contents were collected and fixed with glutaraldehyde (2% final concentration) for 15
566 minutes. Cell abundance in each ISCA treatment (n=5) was quantified by running a
567 standardized volume of sample (50 μl) by flow cytometry as described above. To quantify the
568 strength of chemotaxis, the chemotactic index *Ic* was calculated by dividing the number of cells
569 present in each treatment by the number of cells present in the filtered seawater control³⁰.

570

571 ***Co-growth experiments***

572 Co-cultures were established between each of the three *Marinobacter* phenotypes (WT, $\Delta cheA$
573 and $\Delta fliC$) and *Synechococcus*. *Marinobacter* were grown on Marine Agar plates (Difco
574 Laboratories, Michigan) for 3 days, single colonies were transferred into Marine Broth and
575 grown overnight (12 h). Cells were washed with sterile f/2 media and diluted 1:100 in f/2. A
576 200 μL aliquot was fixed with glutaraldehyde and stained with SYBR Green for enumeration

577 via flow cytometry as described above. *Synechococcus* from a 7-day culture were also diluted
578 1:100 in f/2 and enumerated using flow cytometry as described above. Co-cultures were then
579 set up by inoculating both *Synechococcus* and *Marinobacter* into fresh f/2 medium at a
580 standardized cell density of ~1,000 cells ml⁻¹ (n=4). Co-cultures were incubated at 23°C on a
581 12:12 h dark:light cycle at ~ 180 µmol photons m⁻² s⁻¹ and shaken every 4 hours (180 rpm for
582 15 min) to keep cells in suspension. Cell densities were then enumerated every day for 12 days
583 using flow cytometry as described above.

584

585 *Statistical analysis*

586 Growth data were analyzed using repeated-measure ANOVA after assessing the normality and
587 sphericity of the data, simple main effect tests were then used to assess if treatments were
588 significantly different at each timepoint (*p*-values were corrected using Bonferroni). The
589 chemotaxis responses of *Marinobacter* were then analyzed using a one-way analysis of
590 variance (ANOVA). As the NanoSIMS data were not normally distributed and/or not
591 homogeneous, Kruskal-Wallis test, followed with pairwise Wilcoxon tests were carried out to
592 test the ¹⁵N and ¹³C of the target cells. All *p* values were corrected using the Benjamini–
593 Hochberg procedure for multiple comparisons. All statistical analyses were carried out in R
594 v4.1.1⁵⁰ and analysis scripts are available on GitHub (<https://github.com/JB-Raina-codes/Synechococcus-paper>).

596

597 *Mathematical model for bacteria-phytoplankton interactions*

598 Modelling chemical microenvironments of *Synechococcus*

599 In order to model the dissolved organic matter (DOM) landscape, individual *Synechococcus*
600 cells were considered as point-wise particles, exuding DOM at a rate *L* (molecules per unit
601 time). We begin by considering the DOM concentration around a single *Synechococcus* cell in
602 an unbounded, quiescent fluid. The exuded molecules diffuse radially and are consumed by
603 bacteria distributed throughout the domain. Owing to the spherical symmetry of the problem,
604 both the DOM concentration, *C(r, t)*, and the bacterial concentration, *B(r, t)*, may be written as
605 functions of distance, *r*, from the *Synechococcus* cell, and time, *t*. The DOM profile varies in
606 space and time according to the diffusion equation¹⁶:

$$\frac{\partial C}{\partial t} = D \nabla^2 C - [4\pi a D B(r, t)] C. \quad (2)$$

607 The first and second terms on the right-hand side of Eq. (2) represent the molecular diffusion
 608 of DOM and the diffusion-limited uptake by bacteria, respectively. Amino acids constitute a
 609 significant fraction of the *Synechococcus* exudates (see Table S2), and given their similar
 610 respective molecular weights, we represent the exudate as a single molecular species.
 611 Glutamate was chosen (diffusivity $D = 608 \mu\text{m}^2\text{s}^{-1}$), since its capacity to elicit chemotaxis is
 612 well-studied³². The second term on the right-hand side of Eq. (2) represents diffusion-limited
 613 consumption of the DOM source by bacteria. The parameter a is the cell radius of
 614 *Marinobacter adhaerens*. The distribution of bacteria, $B(r, t)$, will in general not be uniform,
 615 and will depend on $C(r, t)$. However, if we assume that bacteria are approximately uniformly
 616 distributed with concentration B_0 , Eq. (2) may be rewritten as:

$$\frac{\partial C}{\partial t} = D \nabla^2 C - kC, \quad (3)$$

617 where the diffusion-limited consumption rate is given by $k = 4\pi a D B_0$. The steady state
 618 solution to Eq. (3) in spherical coordinates, which is finite at $r \rightarrow \infty$, is given by

$$C(r) = \frac{A}{r} \exp\left(-\sqrt{\frac{k}{D}} r\right) = \frac{A}{r} \exp(-\sqrt{4\pi a B_0} r), \quad (4)$$

619 where $A > 0$ is an arbitrary constant. The radial flux of DOM through a spherical surface at
 620 $r = \epsilon \ll 1$ must match the leakage rate from the *Synechococcus* cell. That is,

$$\lim_{r \rightarrow 0} \left(-D \frac{dC}{dr} 4\pi r^2 \right) = 4\pi A D = L. \quad (5)$$

621 It follows that

$$C(r) = \frac{L}{4\pi D r} \exp(-\sqrt{4\pi a B_0} r). \quad (6)$$

622 Note that the above expression diverges at $r \rightarrow 0$. However, for any bacterium in the vicinity
 623 of the DOM source, the maximum concentration of DOM it may experience occurs at the
 624 surface of *Synechococcus* (with radius $r_0 = 1 \mu\text{m}$). The DOM profile is therefore capped by
 625 this value, so that

$$C(r) = \begin{cases} \frac{L}{4\pi D r_0} \exp(-\sqrt{4\pi a B_0} r_0), & r \leq r_0 \\ \frac{L}{4\pi D r} \exp(-\sqrt{4\pi a B_0} r), & r > r_0 \end{cases} \quad (7)$$

626 We note that the total amount of DOM present in the domain, $\int C(r)dV$, is finite, as the
627 phytoplankton leakage is balanced by bacterial consumption. It is possible to recover the DOM
628 profile in the absence of bacterial consumption by setting $B_0 = 0$. The resulting functional
629 form, $C(r) = L/4\pi Dr$, is used elsewhere¹² in the case of single hotspots. However, for a
630 suspension of *Synechococcus* cells, the long-range nature of this function results in a divergent
631 DOM concentration. It is therefore necessary to utilize the more realistic profile shown in Eq.
632 (7), which encompasses the effect of bacterial consumption. For the purposes of calculating
633 the DOM profile in Eq. (7), the experimental value of $B_0 = 10^6$ cells ml⁻¹ is used.

634

635 The DOM profile presented in Eq. (6) assumes an infinite bacterial suspension surrounding an
636 individual *Synechococcus* cell. We explicitly examine the role that diffusion-limited uptake
637 has in shaping the DOM profile (Extended Data Figure 4a). For four different bacterial
638 concentrations, B_0 (cells ml⁻¹), the DOM profile is shown. Dilutions by factor 2 and 5 from the
639 experimental concentration of $B_0 = 10^6$ cells ml⁻¹ only slightly affect the resultant DOM
640 profile.

641

642 We also test the effect of truncating bacterial density beyond a critical radius, so that $B = B_0$
643 for $r < R_0$ and $B = 0$ beyond this radius. This is essential for assessing the role of interacting
644 phycospheres, where the background concentration of bacteria would not necessarily exhibit
645 the same diffusion-limited uptake for multiple patches simultaneously. Extended Data Figure
646 4b shows the exact solution to Eq. (2) with a step change in bacterial concentration outlined
647 above. Both the dark green curve (bacteria everywhere: $R_0 = \infty$) and black curve (no bacteria:
648 $R_0 = 0$) are identical to those presented in panel A. Truncating the bacterial concentration to
649 lie only in $R_0 < 1000$ μm and $R_0 < 500$ μm barely modifies the DOM concentration profile.
650 In other words, the uptake of DOM by bacteria in the far field is not significant for regulating
651 the DOM profile in the vicinity of the phytoplankton cell. As a result, we are able to directly
652 apply Eq. (6) for a 3D suspension of multiple *Synechococcus* cells.

653

654 Model for multiple resources

655 To mimic the experimental system, we considered a rectangular box with dimensions
656 $l_x = l_y = l_z = l$ in the x, y, z directions respectively. This box is seeded with N identical DOM
657 sources at random positions in space $\{\mathbf{x}_i = (x_i, y_i, z_i) | i = 1, 2, \dots, N\}$, so that the total
658 concentration of *Synechococcus* cells is $\rho = N/l^3$. In all simulations conducted, we set $N =$

659 250, and vary ρ by changing the dimensions of the box, l . Linearity of the diffusion equation
 660 enables the superposition of multiple solutions from Eq. (7). It follows that the total DOM
 661 concentration at position \mathbf{x} is given by

$$C(\mathbf{x}) = \sum_{i=1}^N C_i(\mathbf{d}_i), \quad (8)$$

662 where C_i is the expression in Eq. (7) and d_i is the distance between points \mathbf{x} and \mathbf{x}_i . We utilise
 663 periodic boundary conditions to evaluate d_i , so that the concentration resulting from each
 664 *Synechococcus* cell is evaluated by taking the shortest distance to it within the periodic domain.
 665 From Eqs. (7) and (8), it is also possible to directly evaluate the spatial gradient of the DOM
 666 field, given by $\nabla C(\mathbf{x})$. A single 2D slice of the DOM profile through the box domain with
 667 *Synechococcus* concentration $\rho = 10^3$ cells ml⁻¹ is shown in Extended Data Figure 6.

668

669 Model for bacterial chemotaxis

670 We introduce bacteria into the three-dimensional DOM field defined by Eq. (8) and investigate
 671 their collective dynamics. The relative performance (DOM exposure) of wild type bacteria
 672 compared to their non-chemotactic or non-motile counterparts is examined. To begin with, we
 673 outline the agent-based model for bacterial chemotaxis. This model incorporates the essential
 674 features of bacterial navigation, and accurately captures the chemotaxis of another marine
 675 bacterium, *Vibrio ordalii*³² responding to dissolved glutamate sources (less than 1% fitting
 676 error). Where possible, we have updated specific model parameters for the case of *M.*
 677 *adhaerens* (see Table S8 for all model parameters).

678

679 In the laboratory frame, the DOM concentration is given by the smooth function $C(\mathbf{x})$. In each
 680 simulation time-step, $\Delta t = 0.10$ s, a bacterium with velocity \mathbf{v} and position \mathbf{x} performs a noisy
 681 measurement of the concentration change in its reference frame, $\partial C_N / \partial t = N(\mu, \sigma^2)$. This
 682 stochastic measurement is normally distributed with mean $\mu = \mathbf{v} \cdot \nabla C$ and standard deviation
 683 $\sigma = \Pi [3C(\mathbf{x}, t)/\pi a D T^3]^{1/2}$, and therefore directly incorporates the fundamental precision
 684 with which a cell can measure the gradient. Here Π is the chemotactic precision factor and T is
 685 the timescale over which the bacteria measure the gradient (see³²). For each bacterium, we
 686 model an internal state variable, $S(t)$, which evolves according to

$$\frac{dS}{dt} = -\frac{S}{t_M} + \kappa N(\mu, \sigma^2), \quad (9)$$

687 where $t_M = 1.3$ s is the adaptation timescale⁵¹ and κ is the effective receptor gain – the receptor
688 gain rescaled by the half-saturation constant (see³²). The cell’s mean run time is modified
689 according to the following equation:

$$\tau(S) = \frac{2\tau_0}{1 + \exp(-\Gamma S)} \quad (10)$$

690 where τ_0 is the mean run time of bacteria in their fully adapted state and Γ is the (constant)
691 dimensionless flagellar motor gain. During each time-step, the probability of reorientation is
692 given by $\Delta t/\tau$. Run-reverse-flick reorientation dynamics were included explicitly using known
693 parameters derived for *Vibrio alginolyticus*⁵², and rotational diffusion with $D_r =$
694 $0.0349 \text{ rad}^2 \text{ s}^{-1}$ perturbed the swimming direction at each time-step. Cell motility occurs in
695 three dimensions, as in experiments, with swimming bacteria subject to periodic boundary
696 conditions. The sensory integration timescale is given as $T = 0.1$ s, the cell radius is taken to
697 be $a = 0.5 \mu\text{m}$, the swimming speed $v = |\mathbf{v}| = 45 \mu\text{m s}^{-1}$, and we use the diffusivity for
698 glutamate, $D = 608 \mu\text{m}^2 \text{ s}^{-1}$. For the WT cells, we utilize the recently measured parameter
699 for *Vibrio ordalii*, $\Pi_{\text{sim}} = 6.6$. Initially seeded randomly within the domain, we simulated the
700 3D motion of 500 bacteria as they respond to the DOM landscape. Within the context of this
701 model, it is straightforward to simulate non-chemotactic ($\Delta cheA$) or non-motile ($\Delta fliC$) mutants
702 by fixing $\tau = \tau_0$ or $v = 0$ respectively. We considered the same concentrations of
703 phytoplankton cells (10^3 , 10^4 and 10^5 cells ml^{-1}) as used in the experiments.

704

705 DOM uptake by model bacteria

706 The bacterial trajectories from the numerical simulations were cross-referenced against the 3D
707 DOM landscape to reveal the time-series of DOM exposure for all model bacteria. Diffusion-
708 limited uptake is proportional to the DOM concentration, and so acts as an effective proxy for
709 actual uptake. We investigate the DOM exposure, averaged over time and across the
710 population, as a function of DOM leakage rate and concentration of phytoplankton. The results
711 in Extended Data Figures 7a and 7b illustrate the results for non-chemotactic ($\Delta cheA$) and
712 chemotactic (WT) cells, respectively. Cells in the $\Delta cheA$ strain swim randomly, and therefore
713 sample all areas of their environment with equal probability. The average DOM exposure is
714 therefore proportional to the product $L \times \rho$ for low hotspot concentrations, a feature reflected
715 in the straight-line level contours of Extended Data Figure 7a. These contours are distorted in
716 the case of WT cells (Extended Data Figure 7b) which are able to respond to chemical gradients
717 and attain a relatively high DOM exposure, particularly at low hotspot concentrations. Figure

718 4 in the main text is calculated by taking the ratio of Extended Data Figures 7b and 7a, directly
719 quantifying the advantage due to chemotaxis.

720

721 We calibrated the leakage rate in the mathematical model using the following method. For each
722 phytoplankton concentration (10^3 , 10^4 and 10^5 cells ml $^{-1}$) and across a fine mesh of L values,
723 we calculated the ratio of the mean DOM uptake for the WT cells compared to the $\Delta cheA$
724 mutants. The value $L = 0.052$ pmol hr $^{-1}$ resulted in the closest agreement between the
725 numerical simulations (Extended Data Figure 2) and experimental measurements (Figure 2b).
726 This value of L was applied in simulations designed to mimic experimental conditions.

727

728 The mathematical model does not simulate the release of ^{13}C -enriched compounds from *M.*
729 *adhaerens*, or subsequent uptake by *Synechococcus* cells. Nevertheless, the dynamic results of
730 the numerical simulations provide insight into the experimental findings of Figure 2c. For
731 $\rho = 10^3$ cells ml $^{-1}$, the ^{13}C uptake is significantly higher for WT cells than for $\Delta cheA$ and $\Delta fliC$
732 strains, demonstrating that bacteria-phytoplankton spatial associations influence the ^{13}C
733 transfer. Interestingly, however, the ^{13}C uptake in *Synechococcus* does not vary significantly
734 with concentration of suspended *Synechococcus* cells, even though the concentration of *M.*
735 *adhaerens* is constant across all treatments (10^6 cells ml $^{-1}$). If the ^{13}C exchange was dominated
736 by bulk background concentration of ^{13}C -enriched *Marinobacter* exudates, then the measured
737 enrichment would decrease with *Synechococcus* concentration, as more cells compete for fixed
738 supply of DOM. Similarly, if *Synechococcus* derived chemical gradients were strong enough
739 to trap bacteria for sustained periods of time, then the ^{13}C enrichment would also be expected
740 to drop with increasing *Synechococcus* concentration, ρ . The insensitivity of the results to ρ is
741 consistent with the physical model of fleeting bacteria-phytoplankton interactions. Since
742 chemotaxis prolongs the bacteria-phytoplankton interactions by only a few seconds on average,
743 the number of bacteria entering and departing a given analysis zone per unit time – and
744 therefore the ^{13}C uptake in *Synechococcus* – is only weakly affected by the *Synechococcus*
745 concentration itself.

746

747 For any individual *Synechococcus* cell, the associated DOM concentration profile converges
748 to zero in the limit as $r \rightarrow \infty$ (see Eq. (7)). However, because the simulation volume contains
749 multiple *Synechococcus* cells, the minimum nutrient concentration in the domain – which is
750 found approximately midway between cells – is non-zero. We examined our simulation data

751 to identify the lowest ('background') concentration in each treatment and found that the range
752 of concentrations is commensurate with average free amino-acid concentrations in the ocean
753 (~10-20 nM average, with concentrations up to 100s or 1000 nM in bloom conditions^{53,54}).

754

755 Specifically, the lowest local nutrient concentration occurs in the treatments with 10^3
756 *Synechococcus* cells ml⁻¹, since the phycospheres are most widely separated. For non-
757 chemotactic cells in this case – which explore the landscape uniformly – simulated bacterial
758 trajectories reveal the average nutrient concentration experienced by bacteria to be 3.7 nM
759 (averaged over the simulation time). Conversely, the maximum value of the background
760 concentration occurs in the treatments with 10^5 *Synechococcus* cells ml⁻¹. We examined the
761 simulation data corresponding to these treatments and found nutrient concentrations of
762 approximately 200 nM, a value that is commensurate with free amino acid concentrations
763 occurring in bloom conditions.

764

765 Bacteria-phytoplankton dynamic interactions

766 The full trajectories of all model bacteria are recorded in the simulations. This facilitates
767 exploration of the dynamic interactions between DOM sources and model bacteria. The region
768 immediately surrounding a phytoplankton cell rich in phytoplankton exudates is known as the
769 phycosphere⁹. The exact definition of the phycosphere remains challenging, since the
770 phycosphere is composed of a wide range of chemicals, with different concentrations and
771 diffusivities, which can be used by bacteria as either growth substrates or signals. One way to
772 operationally define the phycosphere is through a threshold DOM concentration compared to
773 the background value¹². Because our work focuses on chemotaxis, we instead define the
774 phycosphere based on the chemotactic properties of WT bacteria, and the behavioral
775 associations with individual phytoplankton. We determine the effective phycosphere radius of
776 the *Synechococcus* cell by examining the behavioral properties of model bacteria as a function
777 of distance from the *Synechococcus* cell. We calculate the residence time, τ , of bacteria within
778 a distance d (μm) of a *Synechococcus* cell. For WT bacteria, the rate at which this residence
779 time increases with d is greatest for $d \leq 35\mu\text{m}$ (Extended Data Figure 3), demonstrating that
780 within this zone, chemotaxis allows bacteria to prolong their spatial association with
781 *Synechococcus*. Conversely, non-chemotactic cells ($\Delta cheA$) exhibit a residence time which
782 grows linearly with d at all distances, with no behavioral biases. We utilize the value $d =$
783 $35\mu\text{m}$ for the phycosphere radius throughout the manuscript. Crucially, the specific choice of

784 phycosphere radius does not influence the total DOM exposure by model bacteria (and does
785 not enter the actual simulations), only the statistics of encounters with phycospheres and time
786 spent within them.

787

788 At every instant in time and for each bacterium, we calculate the distance to the nearest hotspot.
789 The results in Extended Data Figure 8a show the time- and population-averaged minimum
790 distance, as a function of DOM leakage rate, L . The leakage rate may be approximated as
791 scaling with cell radius according to $L \propto r^{2.28}$ ^{55,56}. By matching the fitted leakage rate for
792 *Synechococcus* ($L = 0.052 \text{ pmol hr}^{-1}$) with its known cell radius (Table S8), leakage rate
793 (horizontal axis of Extended Data Figure 8a) can instead be recast in terms of cell radius. As
794 the leakage rate L is increased, WT bacteria are increasingly able to detect and respond to the
795 chemical gradients, resulting in closer physical association with the phytoplankton cells. The
796 grey vertical line in Extended Data Figure 8a corresponds to the fitted value $L = 0.052 \text{ pmol}$
797 hr^{-1} .

798

799 Extended Data Figure 8b displays the percentage of the bacterial population within a distance
800 of $35 \mu\text{m}$ from a hotspot. The role of chemotaxis is clear, with the fraction of cells co-localized
801 with DOM sources increasing dramatically with DOM leakage rate. At the highest leakage rate
802 studied, more than 85% of chemotactic bacteria are within $35 \mu\text{m}$ of a phytoplankton cell. This
803 percentage plateaus at a value less than 100% since the stochastic nature of bacterial run-
804 reverse-flick motion (mean run distance $\sim 21 \mu\text{m}$) precludes a cell from residing indefinitely
805 within the analysis zone.

806

807 **Data availability**

808 All chemotaxis, growth, metabolomics and NanoSIMS data are available in Zenodo
809 (<https://zenodo.org/record/7509161#.Y7fUcRVBw2w>); DOI: 10.5281/zenodo.7509161

810

811 **Code availability**

812 All analysis scripts are available on GitHub (<https://github.com/JB-Rainacodes/Synechococcus-paper>)

814

815 **Acknowledgements**

816 The authors thank F. Carrara and A. Hein for useful discussions. This work was supported by
817 an Australian Research Council grant (DP180100838) to J.R.S. and J.B.R. J.B.R was supported
818 by an Australian Research Council Fellowship (FT210100100). D.R.B. was supported by an
819 Australian Research Council Fellowship (DE180100911). D.R.B. performed simulations using
820 The University of Melbourne's High-Performance Computer *Spartan*
821 (doi.org/10.4225/49/58ead90dceaaa). R.S. acknowledges support from a grant by the Simons
822 Foundation (542395) as part of the Principles of Microbial Ecosystems Collaborative (PriME),
823 a Gordon and Betty Moore Symbiosis in Aquatic Ecosystems Initiative Investigator Award
824 (GBMF9197; <https://doi.org/10.37807/GBMF9197>) and a grant from the Swiss National
825 Science Foundation (315230_176189). We acknowledge use of the Microscopy Australia Ion
826 Probe Facility at The University of Western Australia, a facility funded by the University, State
827 and Commonwealth Governments.

828

829 **Author contributions**

830 J.B.R, D.R.B, S.S., R.S and J.R.S. designed the experiments. M.G. and J.B.R. conducted the
831 experimental work. M.G., P.L.C., P.G., J.B. conducted the NanoSIMS work. J.B.R. and H.M.
832 conducted the metabolomics. D.R.B. conducted the agent-based simulations. E.C.S. and
833 M.S.U. provided the bacterial strains and mutants. J.B.R., D.R.B, R.S and J.R.S. wrote the
834 manuscript and all authors edited subsequent versions.

835

836 **Competing interests**

837 The authors declare no competing interests.

838

839 **Figures captions**

840

841 **Figure 1: Reciprocal exchanges between *Synechococcus* and *Marinobacter adhaerens***
842 **HP15.** (a) Representative $^{15}\text{N}/^{14}\text{N}$ ratio image using NanoSIMS (highlighting the highly
843 enriched *Synechococcus* cell, pink; at least 20 images were acquired per treatment; scale bar:
844 1 μm), (b) ^{15}N uptake of *M. adhaerens* HP15 wild type (WT) originating from *Synechococcus*
845 (10^3 : $n=166$; 10^4 : $n=286$; 10^5 : $n=172$). (c) Representative $^{13}\text{C}/^{12}\text{C}$ ratio image using NanoSIMS
846 (identifying highly enriched *Marinobacter adhaerens* cells, pink; at least 20 images were
847 acquired per treatment; scale bar: 1 μm), and (d) ^{13}C uptake in *Synechococcus* cells originating
848 from *M. adhaerens* (10^3 : $n=10$; 10^4 : $n=17$; 10^5 : $n=37$), at different *Synechococcus*
849 concentrations. (e) Reciprocal exchange of chemical currencies through diffusion in the bulk.
850 Stable isotope uptake from (b) and (d) were calculated according to⁴⁷ (see equation (1) in the
851 Methods). Error bars in (b) and (d) represent standard error of the mean. Significant differences
852 (Kruskal-Wallis) are indicated by using different letters, see also Tables S1 and S3. The full
853 distribution of the data is presented in Extended Data Figure 9.

854

Figure 2: Reciprocal exchanges between *Synechococcus* and *Marinobacter adhaerens* HP15 are enhanced by chemotaxis. (a) The chemotactic (WT), non-chemotactic ($\Delta cheA$) and non-motile ($\Delta fliC$) strains of *Marinobacter* interact with *Synechococcus* phycospheres in qualitatively different ways, resulting in strong differences in the (b) ^{15}N uptake of *M. adhaerens* (10^3 : $n=166$; 10^4 : $n=286$; 10^5 : $n=172$) and (c) ^{13}C uptake in *Synechococcus* (10^3 : $n=10$; 10^4 : $n=17$; 10^5 : $n=37$). Error bars in (b) and (c) represent standard error of the mean. Significant differences (Kruskal-Wallis) are indicated using different letters (see also Tables S6-7). Stable isotope uptake from (c) and (d) were calculated according to⁴⁷ (see equation (1) in the Methods). The full distribution of the data is presented in Extended Data Figure 9.

864

Figure 3: Numerical simulations reveal the dynamic interactions between *Marinobacter* and *Synechococcus*. (a) The duration of every bacterium-phytoplankton interaction (residence time τ) was recorded throughout the simulations, (b) revealing that WT *M. adhaerens* cells spend, on average, more than 3 times longer within each phycosphere ($R_p = 35 \mu\text{m}$) than chemotaxis-deficient mutants (WT: 3.2 ± 11.5 s; $\Delta cheA$: 1.0 ± 1.4 s). For WT cells, 0.58% of encounters were for more than 60 s, while the longest residence time for $\Delta cheA$ cells was 23 s ($n=2626$ encounters). (c) Mean residence time as a function of leakage rate L (or equivalently phytoplankton radius) for three *Synechococcus* concentrations (10^3 dotted, 10^4 dashed, 10^5 solid). (d) The number of unique phytoplankton encounter per day depended strongly on the bacterial motility strategy (mean WT: 12.6 day^{-1} ; $\Delta cheA$: 4.1 day^{-1}). (e) The mean rate of unique phytoplankton encounters as a function of phytoplankton leakage rate and cell concentration for the WT simulations. (f) Bacterial trajectories for three different phytoplankton radii, (i) $R = 0.36 \mu\text{m}$ ($L = 0.1L_0$), (ii) $R = 1 \mu\text{m}$ ($L = L_0$), (iii) $R = 2.7 \mu\text{m}$ ($L = 10L_0$), where L_0 is the value for *Synechococcus*. Bacterial trajectories are colour-coded based on the instantaneous distance to the nearest phytoplankton cell.

880

Figure 4: DOM enhancement due to chemotaxis depends strongly on the size and concentration of phytoplankton cells. (a) The relative DOM exposure (ratio) for chemotactic bacteria (WT) compared to non-chemotactic mutants ($\Delta cheA$) as a function of phytoplankton size (controlled through the leakage rate, L), and phytoplankton concentration. Grey circles correspond to the experimental treatments in Figures 1 and 2. Roman numeral placement in the parameter space correspond to image panels. (b) Schematic representation of phytoplankton sizes and densities depicted by the Roman numerals in (a).

888

889

890 Extended Data Figures

891

Extended Data Figure 1: Chemotactic response of *Marinobacter adhaerens* HP15 to metabolites exuded by *Synechococcus*. The chemotactic index, I_c denotes the concentration of cells within ISCA wells, normalized by the mean concentration of cells within wells containing no chemoattractants (filtered ESAW), after 30 min laboratory deployment. Wells containing *Synechococcus* exudates (1 mg ml^{-1}) and 10% Marine Broth (MB) contained significantly more bacteria than the ESAW control (ANOVA, $n = 5$ biologically independent samples, $p < 0.005$; Table S5). Error bars represent standard error of the mean.

899

Extended Data Figure 2: Dissolved Organic Matter (DOM) exposure of model bacteria. Mean DOM exposure for three bacterial motility strategies across three different *Synechococcus* concentrations (leakage rate $L = 0.052 \text{ pmol hr}^{-1}$). Chemotaxis conferred an enhancement in the DOM exposure by 2.1-, 1.3-, and 1.1-fold, for *Synechococcus*

904 concentrations of 10^3 , 10^4 , and 10^5 cells ml^{-1} respectively, compared to non-chemotactic
905 (ΔcheA) or non-motile (ΔfliC) mutants.

906
907 **Extended Data Figure 3: Residence time of model bacteria.** (a) The bacterial residence
908 time depends on the radius of the analysis zone and motility strategy. For ΔcheA mutants, the
909 residence time grows linearly with radius. However, WT cells exhibit a steep increase for small
910 radii, reflecting their capacity to detect the phytoplankton exudates. (b) The rate at which the
911 residence time increases with radius reveals the zone in which chemotactic bacteria exhibit the
912 strongest behavioral response to the DOM gradient. From this the encounter radius of $35 \mu\text{m}$
913 can be extracted. Other model parameters include $L = 0.052 \text{ pmol hr}^{-1}$, $\rho = 10^3 \text{ cells ml}^{-1}$.
914

915 **Extended Data Figure 4: DOM profile does not depend strongly on bacterial**
916 **consumption.** In each plot, the steady state DOM profile emerges due to a balance between
917 constant phytoplankton exudation and diffusion-limited uptake by bacteria. (a) DOM profile
918 for four different bacterial concentrations. (b) Restricting bacteria to lie in the region $R < R_0$
919 has a minor influence on the resultant DOM profile.
920

921 **Extended Data Figure 5: Growth of *Synechococcus* sp. CS-94 RRIMP N1 and**
922 ***Marinobacter adhaerens* HP15.** (a) Growth curves of *M. adhaerens* HP15 wild type (WT),
923 non-chemotactic mutant (ΔcheA), and non-motile mutant (ΔfliC), each separately co-cultured
924 with *Synechococcus* at an initial concentration of $10^3 \text{ cells ml}^{-1}$ for both partners. (b)
925 Simultaneous growth curve of *Synechococcus* for the same three co-culture experiments. Note:
926 to clearly visualise differences in cell numbers during early timepoints, *Synechococcus* cell
927 numbers are plotted on a logarithmic scale. Asterisks indicate timepoints at which treatments
928 are significantly different (simple main effect test, $p < 0.05$, Table S9). Error bars represent
929 standard error of the mean ($n = 4$ biologically independent samples). (c) Growth curves of
930 *Marinobacter adhaerens* HP15 wild type (WT), non-chemotactic mutant (ΔcheA), and non-
931 motile mutant (ΔfliC) in Marine Broth. Error bars represent standard error of the mean ($n = 3$
932 biologically independent samples). Asterisks indicate timepoints at which treatments are
933 significantly different (simple main effect test, $p < 0.05$, Table S10).
934

935 **Extended Data Figure 6: DOM concentration within a 2D cross-section of the full 3D**
936 **profile.** Results correspond to a *Synechococcus* concentration of $\rho = 10^3 \text{ cells ml}^{-1}$. Other
937 parameters as in Table S8. The white scale bar represents 1 mm.
938

939 **Extended Data Figure 7: DOM exposure of model bacteria.** The mean DOM concentration
940 experienced by (a) non-chemotactic (ΔcheA) mutants and (b) chemotactic (WT) bacteria, as a
941 function of phytoplankton concentration (cells ml^{-1}) and DOM leakage rate L (pmol hr^{-1}).
942

943 **Extended Data Figure 8: Phytoplankton exudation rate affects bacteria-phytoplankton**
944 **distances and bacterial “trapping”.** (a) Bacteria-phytoplankton distance is strongly affected
945 by phytoplankton exudation rate. These data show the distance to the nearest hotspot, averaged
946 over time (3 h co-incubation) and bacterial population (500 cells), as a function of DOM
947 leakage rate L (pmol hr^{-1}). Results are shown for three different phytoplankton concentrations,
948 10^3 (dotted), 10^4 (dashed), $10^5 \text{ cells ml}^{-1}$ (solid), and for three different bacterial mutants:
949 chemotactic WT (blue), non-chemotactic ΔcheA (orange), non-motile ΔfliC (red). (b) Bacteria-
950 phytoplankton trapping statistics. These data show the percentage of bacterial cells that are
951 situated within $35 \mu\text{m}$ of a phytoplankton cell (phycosphere), as a function of DOM leakage
952 rate L (pmol hr^{-1}). For each datapoint, results have been averaged over time (3 h co-incubation)
953 and bacterial population (500 cells). Results are shown for three different phytoplankton

954 concentrations, 10^3 (dotted), 10^4 (dashed), 10^5 cells ml⁻¹ (solid), and for three different bacterial
955 mutants: chemotactic WT (blue), non-chemotactic $\Delta cheA$ (orange), non-motile $\Delta fliC$ (red).

956
957 **Extended Data Figure 9: Distribution of the single cell uptake data reported in Figure 1**
958 and **2.** (a) ^{15}N uptake of *M. adhaerens* (10^3 : n=166; 10^4 : n=286; 10^5 : n=172) and (b) ^{13}C
959 uptake of *Synechococcus* (10^3 : n=10; 10^4 : n=17; 10^5 : n=37).

960
961 **References**

- 962
963 1 Aylward, F. O. *et al.* Microbial community transcriptional networks are conserved in
964 three domains at ocean basin scales. *Proceedings of the National Academy of Sciences*
965 **112**, 5443-5448, doi:10.1073/pnas.1502883112 (2015).
966 2 Fuhrman, J. A. Microbial community structure and its functional implications. *Nature*
967 **459**, 193-199, doi:10.1038/nature08058 (2009).
968 3 Amin, S. A., Parker, M. S. & Armbrust, E. V. Interactions between Diatoms and
969 Bacteria. *Microbiology and Molecular Biology Reviews* **76**, 667-684,
970 doi:10.1128/mmbr.00007-12 (2012).
971 4 Mayali, X. Metabolic Interactions Between Bacteria and Phytoplankton. *Frontiers in*
972 *Microbiology* **9**, doi:10.3389/fmicb.2018.00727 (2018).
973 5 Amin, S. A. *et al.* Photolysis of iron–siderophore chelates promotes bacterial–algal
974 mutualism. *Proceedings of the National Academy of Sciences* **106**, 17071-17076,
975 doi:10.1073/pnas.0905512106 %J Proceedings of the National Academy of Sciences
976 (2009).
977 6 Amin, S. A. *et al.* Interaction and signalling between a cosmopolitan phytoplankton and
978 associated bacteria. *Nature* **522**, 98, doi:10.1038/nature14488 (2015).
979 7 Durham, B. P. *et al.* Cryptic carbon and sulfur cycling between surface ocean plankton.
980 *Proceedings of the National Academy of Sciences* **112**, 453 (2015).
981 8 Stocker, R. Marine microbes see a sea of gradients. *Science* **338**, 628,
982 doi:10.1126/science.1208929 (2012).
983 9 Bell, W. & Mitchell, R. Chemotactic and growth responses of marine bacteria to algal
984 extracellular products. *Biological Bulletin* **143**, 265-277, doi:10.2307/1540052 (1972).
985 10 Azam, F. & Ammerman, J. W. in *Flows of energy and materials in marine ecosystems*
986 345-360 (Springer, 1984).
987 11 Mitchell, J. G., Okubo, A. & Fuhrman, J. A. Microzones surrounding phytoplankton
988 form the basis for a stratified marine microbial ecosystem. *Nature* **316**, 58-59 (1985).
989 12 Seymour, J. R., Amin, S. A., Raina, J.-B. & Stocker, R. Zooming in on the phycosphere:
990 the ecological interface for phytoplankton–bacteria relationships. *Nature Microbiology*
991 **2**, 17065, doi:10.1038/nmicrobiol.2017.65 (2017).
992 13 Sonnenschein, E. C., Syit, D. A., Grossart, H.-P. & Ullrich, M. S. Chemotaxis of
993 *Marinobacter adhaerens* and its impact on attachment to the diatom *Thalassiosira*
994 *weissflogii*. *Applied and Environmental Microbiology* **78**, 6900-6907,
995 doi:10.1128/aem.01790-12 (2012).
996 14 Raina, J.-B., Fernandez, V., Lambert, B., Stocker, R. & Seymour, J. R. The role of
997 microbial motility and chemotaxis in symbiosis. *Nature Reviews Microbiology* **17**, 284-
998 294, doi:10.1038/s41579-019-0182-9 (2019).
999 15 Seymour, J. R., Ahmed, T., Durham, W. M. & Stocker, R. Chemotactic response of
1000 marine bacteria to the extracellular products of *Synechococcus* and *Prochlorococcus*.
1001 *Aquatic Microbial Ecology* **59**, 161-168 (2010).
1002 16 Smriga, S., Fernandez, V. I., Mitchell, J. G. & Stocker, R. Chemotaxis toward
1003 phytoplankton drives organic matter partitioning among marine bacteria. *Proceedings*

- 1004 of the National Academy of Sciences **113**, 1576-1581, doi:10.1073/pnas.1512307113
1005 (2016).

1006 17 Flombaum, P., Wang, W.-L., Primeau, F. W. & Martiny, A. C. Global
1007 picophytoplankton niche partitioning predicts overall positive response to ocean
1008 warming. *Nature Geoscience* **13**, 116-120, doi:10.1038/s41561-019-0524-2 (2020).

1009 18 Christie-Oleza, J. A., Sousoni, D., Lloyd, M., Armengaud, J. & Scanlan, D. J. Nutrient
1010 recycling facilitates long-term stability of marine microbial phototroph-heterotroph
1011 interactions. *Nature Microbiology* **2**, 17100, doi:10.1038/nmicrobiol.2017.100 (2017).

1012 19 Morris, J. J., Kirkegaard, R., Szul, M. J., Johnson, Z. I. & Zinser, E. R. Facilitation of
1013 robust growth of *Prochlorococcus* colonies and dilute liquid cultures by “helper”
1014 heterotrophic bacteria. *Applied and Environmental Microbiology* **74**, 4530-4534,
1015 doi:10.1128/aem.02479-07 (2008).

1016 20 Sher, D., Thompson, J. W., Kashtan, N., Croal, L. & Chisholm, S. W. Response of
1017 *Prochlorococcus* ecotypes to co-culture with diverse marine bacteria. *The ISME
1018 Journal* **5**, 1125-1132, doi:10.1038/ismej.2011.1 (2011).

1019 21 Aharonovich, D. & Sher, D. Transcriptional response of *Prochlorococcus* to co-culture
1020 with a marine *Alteromonas*: differences between strains and the involvement of putative
1021 infochemicals. *The ISME Journal* **10**, 2892-2906, doi:10.1038/ismej.2016.70 (2016).

1022 22 Jackson, G. A. Simulating chemosensory responses of marine microorganisms.
1023 *Limnology and Oceanography* **32**, 1253-1266, doi:10.4319/lo.1987.32.6.1253 (1987).

1024 23 Gärdes, A., Iversen, M. H., Grossart, H.-P., Passow, U. & Ullrich, M. S. Diatom-
1025 associated bacteria are required for aggregation of *Thalassiosira weissflogii*. *The ISME
1026 Journal* **5**, 436-445, doi:10.1038/ismej.2010.145 (2011).

1027 24 Al-Wahaib, D., Al-Bader, D., Al-Shaikh Abdou, D. K., Eliyas, M. & Radwan, S. S.
1028 Consistent occurrence of hydrocarbonoclastic *Marinobacter* strains in various cultures
1029 of picocyanobacteria from the Arabian Gulf: promising associations for biodegradation
1030 of marine oil pollution. *Journal of Molecular Microbiology and Biotechnology* **26**, 261-
1031 268, doi:10.1159/000445686 (2016).

1032 25 Raina, J.-B. et al. Subcellular tracking reveals the location of
1033 dimethylsulfoniopropionate in microalgae and visualises its uptake by marine bacteria.
1034 *eLife* **6**, e23008, doi:10.7554/eLife.23008 (2017).

1035 26 Brumley, D. R. et al. Cutting through the noise: bacterial chemotaxis in marine
1036 microenvironments. *Frontiers in Marine Science* **7**, doi:10.3389/fmars.2020.00527
1037 (2020).

1038 27 Gärdes, A. et al. Complete genome sequence of *Marinobacter adhaerens* type strain
1039 (HP15), a diatom-interacting marine microorganism. *Standards in Genomic Sciences*
1040 **3**, 97-107, doi:10.4056/sigs.922139 (2010).

1041 28 Moore, L. R., Post, A. F., Rocap, G. & Chisholm, S. W. Utilization of different nitrogen
1042 sources by the marine cyanobacteria *Prochlorococcus* and *Synechococcus*. *Limnology
1043 and Oceanography* **47**, 989-996, doi:10.4319/lo.2002.47.4.0989 (2002).

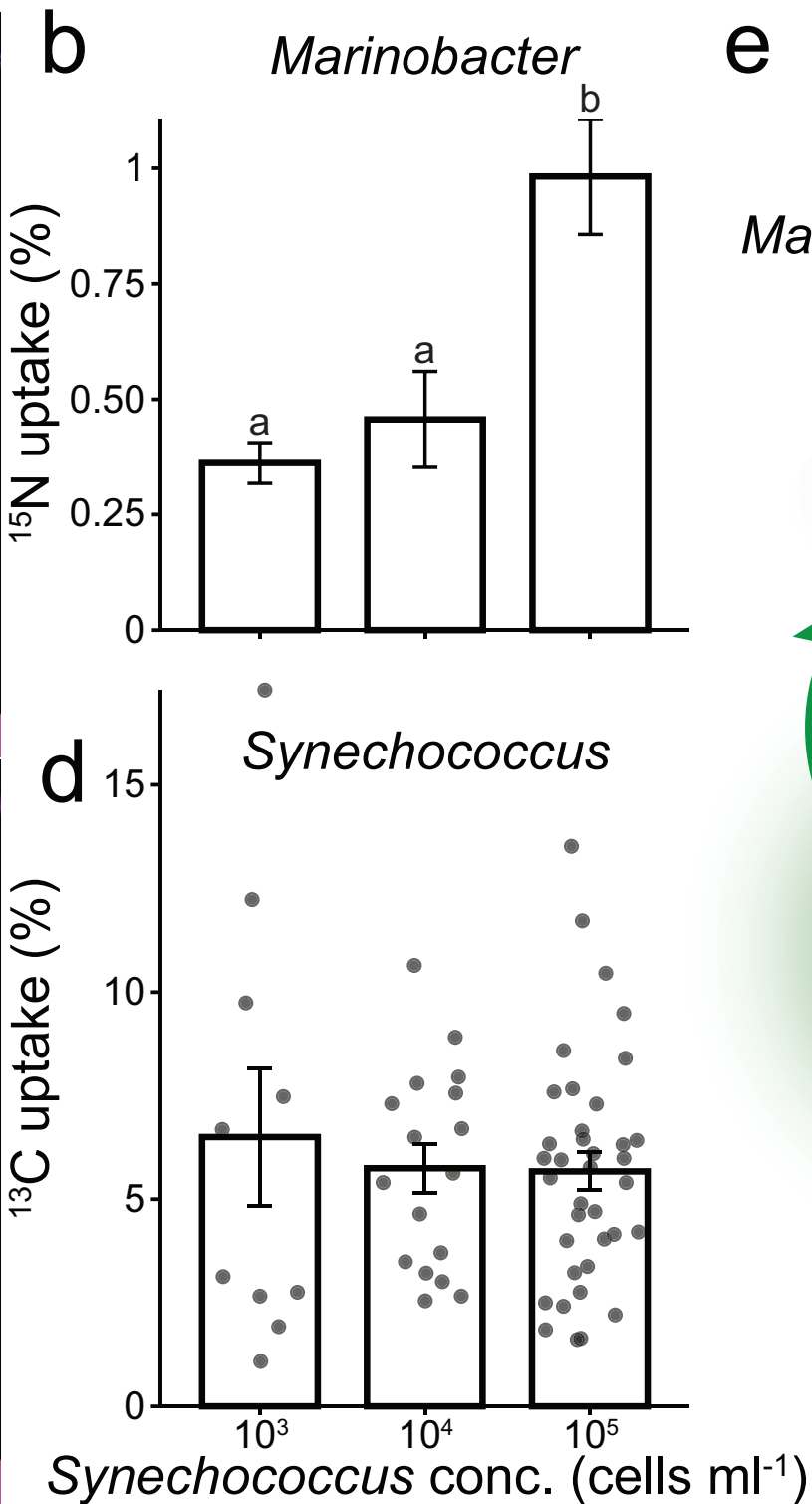
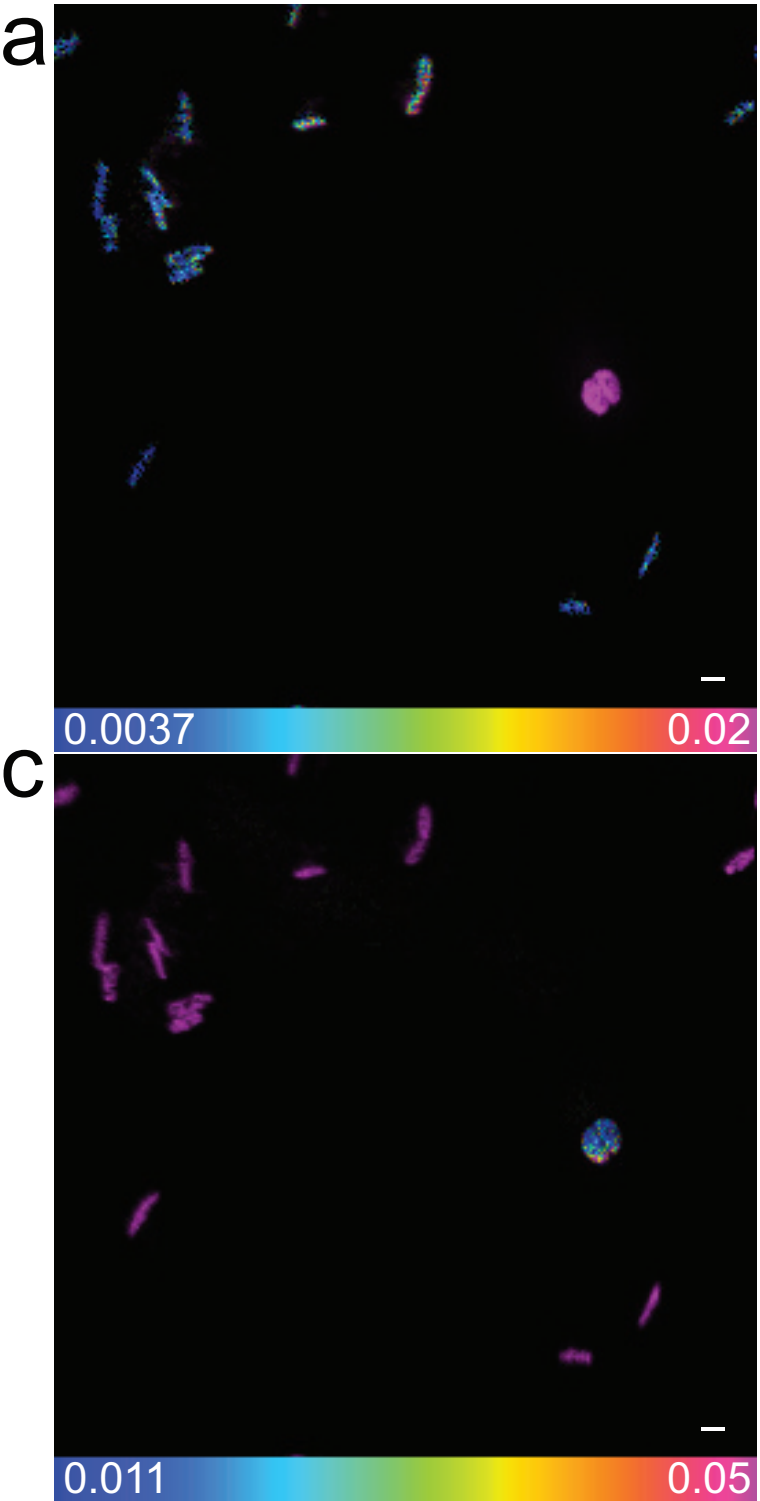
1044 29 Wawrik, B., Callaghan, A. V. & Bronk, D. A. Use of inorganic and organic nitrogen
1045 by *Synechococcus* spp. and Diatoms on the West Florida shelf as measured using stable
1046 isotope probing. *Applied and Environmental Microbiology* **75**, 6662-6670,
1047 doi:10.1128/aem.01002-09 (2009).

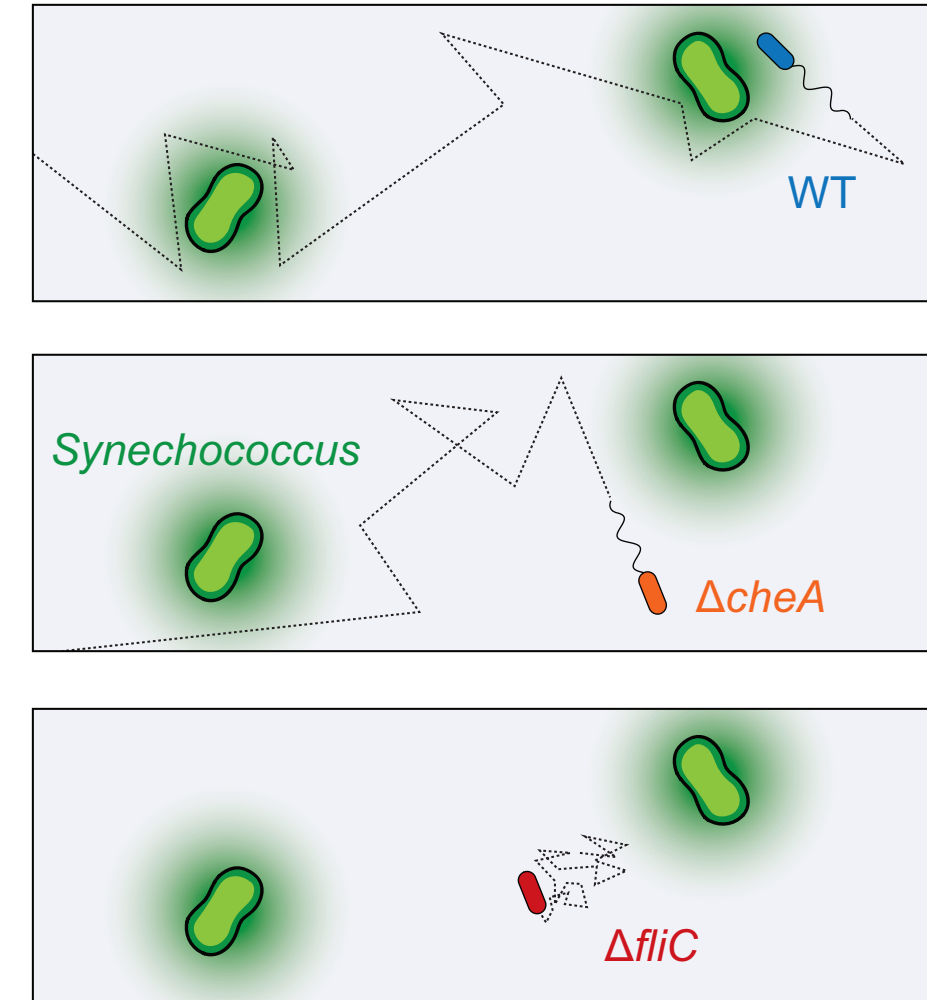
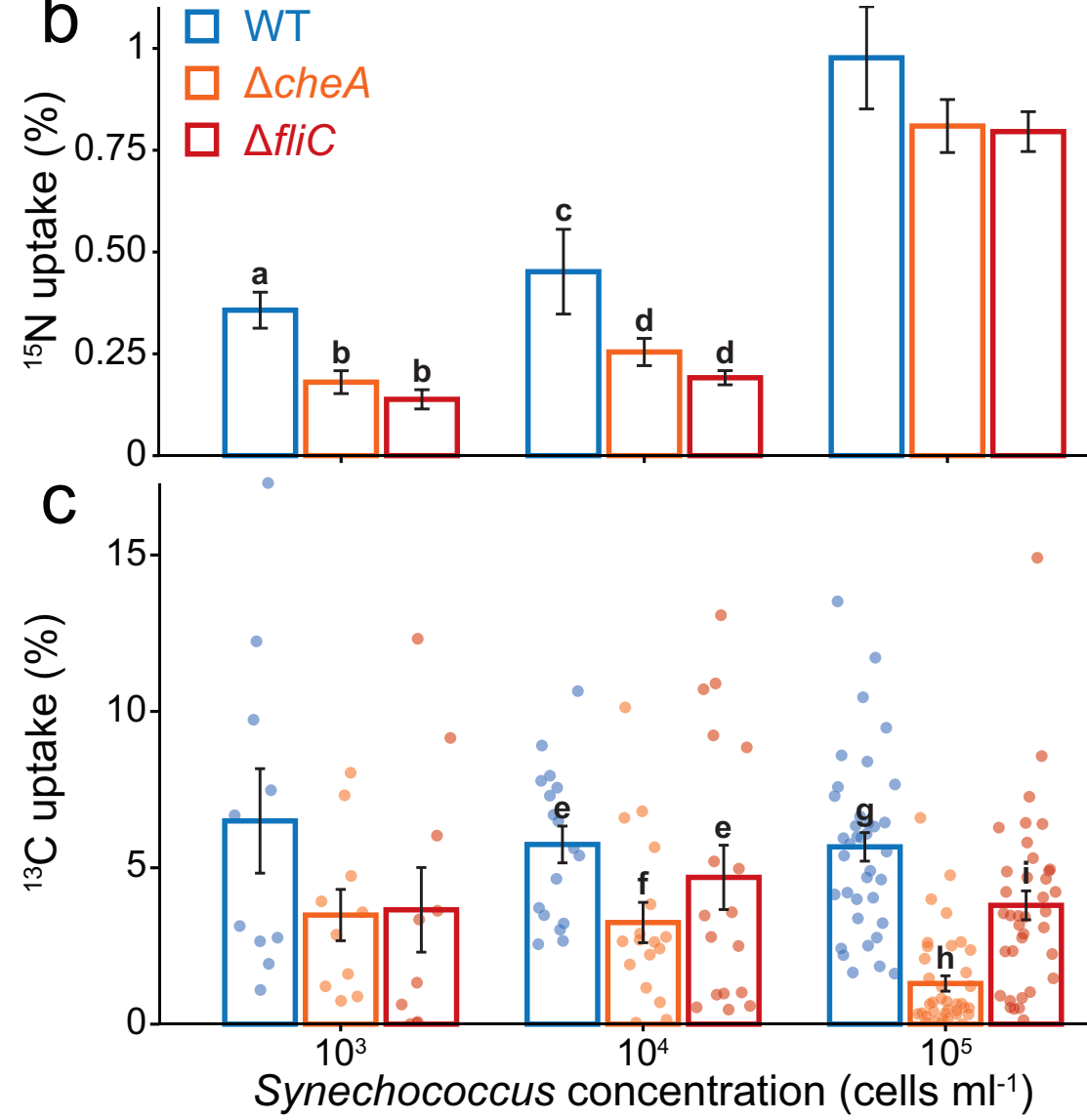
1048 30 Lambert, B. S. et al. A microfluidics-based in situ chemotaxis assay to study the
1049 behaviour of aquatic microbial communities. *Nature Microbiology* **2**, 1344-1349,
1050 doi:10.1038/s41564-017-0010-9 (2017).

1051 31 Raina, J.-B. et al. Chemotaxis shapes the microscale organization of the ocean’s
1052 microbiome. *Nature* **605**, 132-138, doi:10.1038/s41586-022-04614-3 (2022).

- 1053 32 Brumley, D. R. *et al.* Bacteria push the limits of chemotactic precision to navigate
1054 dynamic chemical gradients. *Proceedings of the National Academy of Sciences* **116**,
1055 10792-10797, doi:10.1073/pnas.1816621116 (2019).
- 1056 33 Myklestad, S. M. in *Marine Chemistry* (ed P. J. Wangersky) 111-148 (Springer Berlin
1057 Heidelberg, 2000).
- 1058 34 Ni, B., Colin, R., Link, H., Endres, R. G. & Sourjik, V. Growth-rate dependent resource
1059 investment in bacterial motile behavior quantitatively follows potential benefit of
1060 chemotaxis. *Proceedings of the National Academy of Sciences* **117**, 595-601,
1061 doi:10.1073/pnas.1910849117 (2020).
- 1062 35 Stocker, R., Seymour, J. R., Samadani, A., Hunt, D. E. & Polz, M. F. Rapid chemotactic
1063 response enables marine bacteria to exploit ephemeral microscale nutrient patches.
1064 *Proceedings of the National Academy of Sciences* **105**, 4209-4214,
1065 doi:10.1073/pnas.0709765105 (2008).
- 1066 36 Buitenhuis, E. *et al.* MAREDAT: towards a world atlas of MARine Ecosystem DATa.
1067 *Earth Syst. Sci. Data* **5**, 227–239 (2013).
- 1068 37 Raina, J.-B. *et al.* Symbiosis in the microbial world: from ecology to genome evolution.
1069 *Biology Open* **7**, bio032524, doi:10.1242/bio.032524 (2018).
- 1070 38 Giardina, M. *et al.* Quantifying Inorganic Nitrogen Assimilation by Synechococcus
1071 Using Bulk and Single-Cell Mass Spectrometry: A Comparative Study. *Frontiers in*
1072 *Microbiology* **9**, doi:10.3389/fmicb.2018.02847 (2018).
- 1073 39 Berges, J. A., Franklin, D. J. & Harrison, P. J. Evolution of an artificial seawater
1074 medium: improvements in enriched seawater, artificial water over the last two decades.
1075 *Journal of Phycology* **37**, 1138-1145, doi:10.1046/j.1529-8817.2001.01052.x (2001).
- 1076 40 Guillard, R. R. L. in *Culture of Marine Invertebrate Animals: Proceedings — 1st*
1077 *Conference on Culture of Marine Invertebrate Animals Greenport* (eds Walter L.
1078 Smith & Matoira H. Chanley) 29-60 (Springer US, 1975).
- 1079 41 Kaeppel, E. C., Gärdes, A., Seebah, S., Grossart, H.-P. & Ullrich, M. S. *Marinobacter*
1080 *adhaerens* sp. nov., isolated from marine aggregates formed with the diatom
1081 *Thalassiosira weissflogii*. *International Journal of Systematic and Evolutionary*
1082 *Microbiology* **62**, 124-128, doi:10.1099/ijss.0.030189-0 (2012).
- 1083 42 Sonnenschein, E. C. *et al.* Development of a genetic system for *Marinobacter*
1084 *adhaerens* HP15 involved in marine aggregate formation by interacting with diatom
1085 cells. *Journal of Microbiological Methods* **87**, 176-183,
1086 doi:10.1016/j.mimet.2011.08.008 (2011).
- 1087 43 Marie, D., Partensky, F., Jacquet, S. & Vaultot, D. Enumeration and cell cycle analysis
1088 of natural populations of marine picoplankton by flow cytometry using the nucleic acid
1089 stain SYBR Green I. *Applied and Environmental Microbiology* **63**, 186-193 (1997).
- 1090 44 Marie, D., Partensky, F., Jacquet, S. & Vaultot, D. Enumeration and cell cycle analysis
1091 of natural populations of marine picoplankton by flow cytometry using the nucleic acid
1092 stain SYBR Green I. **63**, 186-193 (1997).
- 1093 45 Schindelin, J. *et al.* Fiji: an open-source platform for biological-image analysis. *Nature*
1094 *Methods* **9**, 676-682, doi:10.1038/nmeth.2019 (2012).
- 1095 46 Hillion, F., Kilburn, M., Hoppe, P., Messenger, S. & Weber, P. K. The effect of QSA
1096 on S, C, O and Si isotopic ratio measurements. *Geochimica et Cosmochimica Acta* **72**,
1097 A377-A377 (2008).
- 1098 47 Popa, R. *et al.* Carbon and nitrogen fixation and metabolite exchange in and between
1099 individual cells of *Anabaena oscillarioides*. *The ISME Journal* **1**, 354-360,
1100 doi:10.1038/ismej.2007.44 (2007).
- 1101 48 Sumner, L. W. *et al.* Proposed minimum reporting standards for chemical analysis.
1102 *Metabolomics* **3**, 211-221, doi:10.1007/s11306-007-0082-2 (2007).

- 1103 49 Clerc, E. E., Raina, J.-B., Lambert, B. S., Seymour, J. & Stocker, R. In Situ Chemotaxis
1104 Assay to Examine Microbial Behavior in Aquatic Ecosystems. *JoVE*, e61062,
1105 doi:doi:10.3791/61062 (2020).
- 1106 50 Ihaka, R. & Gentleman, R. R: A Language for Data Analysis and Graphics. *Journal of
1107 Computational and Graphical Statistics* **5**, 299-314,
1108 doi:10.1080/10618600.1996.10474713 (1996).
- 1109 51 Xie, L., Lu, C. & Wu, X.-L. Marine bacterial chemoresponse to a stepwise
1110 chemoattractant stimulus. *Biophysical Journal* **108**, 766-774,
1111 doi:10.1016/j.bpj.2014.11.3479 (2015).
- 1112 52 Son, K., Guasto, J. S. & Stocker, R. Bacteria can exploit a flagellar buckling instability
1113 to change direction. *Nature Physics* **9**, 494-498, doi:10.1038/nphys2676 (2013).
- 1114 53 Lee, C. & Bada, J. L. Amino acids in equatorial Pacific Ocean water. *Earth and
1115 Planetary Science Letters* **26**, 61-68, doi:[https://doi.org/10.1016/0012-
1116 821X\(75\)90177-6](https://doi.org/10.1016/0012-821X(75)90177-6) (1975).
- 1117 54 Yamashita, Y. & Tanoue, E. Distribution and alteration of amino acids in bulk DOM
1118 along a transect from bay to oceanic waters. *Marine Chemistry* **82**, 145-160,
1119 doi:[https://doi.org/10.1016/S0304-4203\(03\)00049-5](https://doi.org/10.1016/S0304-4203(03)00049-5) (2003).
- 1120 55 Menden-Deuer, S. & Lessard, E. J. Carbon to volume relationships for dinoflagellates,
1121 diatoms, and other protist plankton. *Limnology and Oceanography* **45**, 569-579,
1122 doi:10.4319/lo.2000.45.3.0569 (2000).
- 1123 56 Mullin, M. M., Sloan, P. R. & Eppley, R. W. Relationship between carbon content, cell
1124 volume and area in phytoplankton. *Limnology and Oceanography* **11**, 307-311,
1125 doi:10.4319/lo.1966.11.2.0307 (1966).
- 1126



a**b****c**